The American Journal of Pathology, Vol. 186, No. 8, August 2016

ELSEVIER

The American Journal of PATHOLOGY

ajp.amjpathol.org

IMMUNOPATHOLOGY AND INFECTIOUS DISEASES

The Complement Regulatory Protein CD46 Deficient Mouse Spontaneously Develops Dry-Type Age-Related Macular Degeneration—Like Phenotype

Valeriy V. Lyzogubov,* Puran S. Bora,* Xiaobo Wu,† Leah E. Horn,*‡ Ryan de Roque,*§ Xeniya V. Rudolf,* John P. Atkinson,† and Nalini S. Bora*‡

From the Department of Ophthalmology, Jones Eye Institute, Pat and Willard Walker Eye Research Center, University of Arkansas for Medical Sciences, Little Rock, Arkansas; the Division of Rheumatology,† Department of Medicine, Washington University School of Medicine, St. Louis, Missouri; the Department of Microbiology and Immunology,‡ University of Arkansas for Medical Sciences, Little Rock, Arkansas; and the University of Arkansas for Medical Sciences,§ College of Medicine, Little Rock, Arkansas*

Accepted for publication March 31, 2016.

Address correspondence to Nalini S. Bora, Ph.D., Department of Ophthalmology, Jones Eye Institute, University of Arkansas for Medical Sciences, 4301 W Markham, 523-7, Little Rock, AR 72205-7199. E-mail: nbora@uams.edu.

In the mouse, membrane cofactor protein (CD46), a key regulator of the alternative pathway of the complement system, is only expressed in the eye and on the inner acrosomal membrane of spermatozoa. We noted that although *Cd46*$^{-/-}$ mice have normal systemic alternative pathway activating ability, lack of CD46 leads to dysregulated complement activation in the eye, as evidenced by increased deposition of C5b-9 in the retinal pigment epithelium (RPE) and choroid. A knockout of CD46 induced the following cardinal features of human dry age-related macular degeneration (AMD) in 12-month-old male and female mice: accumulation of autofluorescent material in and hypertrophy of the RPE, dense deposits in and thickening of Bruch's membrane, loss of photoreceptors, cells in subretinal space, and a reduction of choroidal vessels. Collectively, our results demonstrate spontaneous age-related degenerative changes in the retina, RPE, and choroid of *Cd46*$^{-/-}$ mice that are consistent with human dry AMD. These findings provide the exciting possibility of using *Cd46*$^{-/-}$ mice as a convenient and reliable animal model for dry AMD. Having such a relatively straight-forward model for dry AMD should provide valuable insights into pathogenesis and a test model system for novel drug targets. More important, tissue-specific expression of CD46 gives the *Cd46*$^{-/-}$ mouse model of dry AMD a unique advantage over other mouse models using knockout strains. *(Am J Pathol 2016, 186: 2088—2104; http://dx.doi.org/10.1016/j.ajpath.2016.03.021)*

Age-related macular degeneration (AMD) is a leading cause of irreversible vision loss in individuals >50 years of age in the United States and around the world.[1—5] This disease causes a progressive destruction of the macula, leading to the loss of central vision. AMD is a chronic degenerative process with multiple risk factors.[2,3,6—17] Nearly two million individuals in the United States alone are currently afflicted with AMD. This number is expected to grow in part because of increasing life expectancy.[5] Clinically, AMD is usually classified into two forms—nonexudative (dry type) and exudative (wet type). Although the dry form of AMD is more prevalent (approximately 85% of the cases) and a precursor to wet AMD, the fundamental processes underlying dry AMD are particularly not well understood.[2—4,6—10] Several agents to treat dry AMD are currently in the developmental stage. However, no effective treatment option is currently available.[11,12] Novel therapeutic targets for dry AMD need to be discovered.

Supported by The Edward N. and Della L. Thome Memorial Foundation grant, Lions of Arkansas Foundation, Inc., grant, the Pat and Willard Walker Eye Research Center grant, and Jones Eye Institute (Little Rock, AR) grant, the Protein Production and Purification Core Facility of the Rheumatic Diseases Core Center under Award P30AR048335, National Institute of Arthritis and Musculoskeletal and Skin Diseases (J.P.A.), National Institute of General Medical Sciences under Award R01 GM099111 (J.P.A.), and National Institute of Allergy and Infectious Diseases under Award R01 AI041592 (J.P.A. and X.W.).

Disclosures: None declared.

The content is solely the responsibility of the authors and does not necessarily represent the official views of the NIH.

http://dx.doi.org/10.1016/j.ajpath.2016.03.021

Studies during the past decade have shown that the alternative pathway (AP) of the complement system is a critical player in AMD pathogenesis. A simple interpretation of the accumulating data from animal and especially human studies is that in AMD there is overactivation of the AP, leading to adverse consequences.[1–4,6,13–28] CD46, the major membrane regulatory protein of the AP in most vertebrate species, except for rodents, is critical for regulation of AP.[29–32] Although expressed widely by human nucleated cells, mouse CD46 was thought to be only present on the inner acrosomal membrane of spermatozoa.[30,31]

Recently, we reported that CD46 is expressed in the neurosensory retina, retinal pigment epithelium (RPE), and choroid of the mouse eye.[28] Our goal was to investigate if the *Cd46*$^{-/-}$ mouse spontaneously develops a phenotype that closely resembles the dry form of human AMD. Herein, we describe that *Cd46*$^{-/-}$ male and female mice have normal systemic AP activating ability, but the lack of ocular CD46 leads to dysregulated complement activation in the retina and choroid. Furthermore, aged *Cd46*$^{-/-}$ mice spontaneously develop cardinal features of human dry AMD.

Materials and Methods

Animals

We have previously described the generation of a mouse with homozygous deficiency of *Cd46* (*Cd46*$^{-/-}$) on the C57BL/6 background.[28] *C3*$^{-/-}$, *Cfb*$^{-/-}$, and *Cfp*$^{-/-}$ mice were generated, as previously reported.[33–35] Mice were bred and housed in a pathogen-free, temperature-controlled environment. Genotyping was performed by PCR analysis using tail-derived DNA. The following primers were used in PCR analysis: CD46, 5′-ATGCCTGTGAACTACCACGGCCATTTGAAG-3′ (forward) and 5′-AACTTTAATATAGCTCCAGTGCCAGTTGCA-3′ (reverse); Neo, 5′-AACAGACAATCGGCTGCTCTGATG-3′ (forward) and 5′-GCTCTTCGTCCAGATCATCCTGATCG-3′ (reverse); C3, 5′-GATCCCCAGAGCTAATG-3′ (V787) and 5′-AGGGACCAGCCCAGGTTCAG-3′ (V789); Neo, 5′-TCGTCCTGCAGTTCATTCAG-3′ (V788); FB, 5′-CCGAAGCATTCCTATCCTCC-3′ (forward 1), 5′-GTAGTCTTGTCTGCTTTCTCC-3′ (reverse 1), and 5′-CGAATGGGTGACCGCTTCC-3′ (Neo).

For properdin (P), the following neoprimers were initially used in PCR analysis: Neo F371, 5′-AACAGACAATCGGCTGCTCTGATG-3′; Neo R779, 5′-GCTCTTCGTCCAGATCATCCTGATCG-3′. Western blotting using rabbit anti-mouse properdin[36] was used to establish the absence of properdin in the *Cfp*$^{-/-}$ mouse.

Protocols for animal breeding, housing, and handling were approved by the Division of Comparative Medicine at Washington University (St. Louis, MO) and Institutional Animal Care and Use Committee, University of Arkansas for Medical Sciences (Little Rock, AR). All mice were kept under a 12-hour dark and 12-hour light cycle with ad libitum access to food and water.

Homozygous *Cd46* knockout mice were backcrossed into C57BL/6 for at least eight generations before use. Male and female C57BL/6 mice were purchased from the Jackson Laboratory (Bar Harbor, ME) and served as a wild-type control.

Sample Collection

Two-month-old (adult) and 12-month-old (aged) mice were used. The eyes from the following eight groups of mice were analyzed: group 1, wild type (WT) male, 2-month-old; group 2, WT female, 2-month-old; group 3, *Cd46*$^{-/-}$ male, 2-month-old; group 4, *Cd46*$^{-/-}$ female, 2-month-old; group 5, WT male, 12-month-old; group 6, WT female, 12-month-old; group 7, *Cd46*$^{-/-}$ male, 12-month-old; and group 8, *Cd46*$^{-/-}$ female, 12-month-old.

Tissue Processing

Eyes for histological investigation were processed as described.[24,26,28] Animals were sacrificed between 4 and 7 hours after the light was turned on using carbon dioxide inhalation, and the eyes were harvested immediately. One eye from each animal was fixed in 4% buffered paraformaldehyde (pH 7.4 in 0.05 mol/L phosphate-buffered saline) and embedded in paraffin. Three composite blocks were formed to contain two eyes from each group (total six eyes from each group) and serial sections (5 μm thick) were cut. Paraffin sections were stained with hematoxylin and eosin or were subsequently used in immunofluorescence (IF) analysis as described below.

One eye from each animal was fixed with 2.5% glutaraldehyde (Polysciences Inc., Warrington, PA) for 1 hour. The anterior part of the eye (including the ciliary body and lens) was removed, whereas the posterior part of the eye was fixed in 2.5% glutaraldehyde for additional 3 hours. Samples were washed in 7.5% sucrose overnight. The posterior part of the eye was sliced in two parts by a sagittal cut close to the optic nerve and post fixed in 1% osmium tetroxide (Polysciences Inc.) in 0.05 mol/L phosphate-buffered saline for 1 hour at room temperature. Samples were then treated with saturated solution of uranyl acetate (Polysciences Inc.) prepared in 50% ethanol for 1 hour at room temperature. Ethanol was used to dehydrate the tissue. Electron microscopy grade acetone (Polysciences Inc.) was used as an intermediate medium between ethanol and resin. The Embed 812 epon resin kit (Electron Microscopy Sciences, Hatfield, PA) was used for embedding. All samples were oriented with sagittal slice facing the cutting surface in silicon molds before polymerization (24 hours at 45°C and 24 hours at 57°C). Semithin (1 μm thick) sections from each plastic block (two blocks per eye) were cut and stained using Toluidine Blue and Basic Fuchsin (Electron Microscopy Sciences) for 1 minute at 60°C, dried, and embedded in Canada balsam (Alfa Aesar, Heysham, England). These stains differentiate basophilic structures (pink) and nuclei (blue). Semithin (1 μm thick) sections were used for light

microscopy, whereas ultrathin (60 to 80 nm thick) sections were used for electron microscopy.

IF Analysis

Serial sections of composite blocks were used in IF studies for membrane attack complex (MAC; C5b-9) and detection of autofluorescence. Using sections containing two eyes from each of the eight groups generated identical conditions for each step and all samples were processed at the same time. Sections were deparaffinized, hydrated, and treated with antigen unmasking solution (Vector Laboratories, Burlingame, CA). For detection of MAC, sections were treated with rabbit polyclonal anti-MAC (C9 neoepitope) antibody (Ab; primary Ab) provided by Prof. B. P. Morgan (University of Wales College of Medicine, Cardiff, UK), followed by AF488-conjugated donkey anti-rabbit IgG (H + L) (Molecular Probes, Eugene, OR). To identify RPE cells on the same sections, we used DyLight 649 conjugated mouse monoclonal anti-RPE65 (IgG1 κ) from Novus Biological (Littleton, CO). Negative control sections were stained with an isotype-matched control Ab at identical concentrations to those of the primary Ab.

To reduce autofluorescence, we treated paraffin sections with 1% Sudan Black after immunostaining as described.[23] To investigate autofluorescence in RPE, sections (not treated with Sudan Black) were mounted in ProLong antifade reagent with DAPI (Invitrogen, Grand Island, NY). Images were captured using the laser confocal microscope LSM510. Beam Splitters were set up as follows: 405-nm laser (10%) window, 20 to 480 nm; 488-nm laser (10%) window, 505 to 530 nm; and 561-nm laser (15%) window, 575 to 615 nm. Eight-bit images were obtained using the microscope in sequential mode with line average of eight and format of 1024 × 1024 pixels for autofluorescence investigation and 512 × 512 pixels for C5b-9 IF. We captured a single 1-μm optical slice of each section stained for C5b-9 using the Plan-Apochromat 40×/1.4 or 63×/1.4 oil differential interference contrast objectives. We obtained a 3-μm optical slice for investigation of autofluorescence using Plan-Apochromat 63×/1.4 oil differential interference contrast objective. All images were captured with the same settings. Differential interference contrast images were captured to facilitate localization of histological structures of the eye. Intensity of C5b-9 positive staining on RPE and choroid was observed by two independent investigators in a masked manner. Integrated (total) intensity of the signal was used to evaluate C5b-9 positive fluorescence. C5b-9 positive fluorescence (green channel) was measured using ImageJ software version 1.50b (NIH, Bethesda, MD) in RPE-choroid. Autofluorescence (red channel) of paraffin sections was measured using ImageJ in RPE65 positive structures.

Angiography

To investigate choroidal vasculature, WT male and *Cd46*$^{-/-}$ male mice (at 2 and 12 months of age) were first anesthetized with ketamine/xylazine cocktail. Animals were then perfused (through the heart) with 0.75 mL of phosphate-buffered saline containing 50 mg/mL of fluorescein isothiocyanate (FITC)-labeled dextran (2 × 10^6 molecular weight; Sigma, St. Louis, MO) before they were sacrificed.[18–20,28] Harvested eyes were dissected, and the posterior part of the eye was gently scratched with a bine brush to destroy RPE cells and remove pigment. Choroid-sclera complexes were flat mounted in ProLong antifade reagent with DAPI (Invitrogen). Z-stack images of flat mounts were captured (in a consistent location), and a three-dimensional model of choroidal vasculature was built using ZEN software version 2009 (Zeiss, Jena, Germany). Area of FITC-dextran perfused choroidal vessels (green color)/total image area was measured using ImageJ. This reflects the density of choroidal vessels.

Microscopy

Hematoxylin and eosin–stained paraffin sections and semithin epon sections were examined using Olympus Vanox-S AH-2 microscope (Olympus Optical, Tokyo, Japan) equipped with a QImaging GO-5 camera (Surrey, BC, Canada). We used 1× objective to capture entire section and 40× and/or 100× oil objective to capture images for morphometry. Each section was divided in four zones using a point between ciliary body and optic nerve. Two peripheral zones and two central zones were defined. Two images were captured from each zone (total eight images per section). One field of view close to optic nerve or ciliary body was excluded from the analysis. Images were captured in areas of RPE-choroid-sclera complex and outer nuclear layer (ONL) with photoreceptor outer segment (POS) and photoreceptor inner segment (PIS). QCapture Pro software version 5.1.1.14 (Media Cybernetics, Bethesda, MD) was used to capture images. For IF analysis, we used a laser confocal microscope LSM510 (Carl Zeiss, Jena).

Electron microscopy was performed using a FEI Tecnai G2 TF20 transmission electron microscope (FEI Worldwide Corporate Headquarters, Hillsboro, OR). We used ×5000 magnification to capture the basal surface of RPE, Bruch's membrane (BM), and choroidal capillaries.

Morphometry

ImageJ was used to measure thickness of the ONL, density of nuclei in the ONL, and total length of PIS and POS. Total length of PIS and POS was measured as a distance between outer limiting membrane and the free end of photoreceptor outer segment facing RPE cells. For each image, length of ONL was measured as a distance between outer margin of ONL and outer limiting membrane. We also determined the density of nuclei in ONL by counting the number of nuclei on the image. These parameters reflect photoreceptor degeneration and loss.

We counted the number of nuclei in RPE cell layer, number of cells in subretinal space, and measured the length of RPE layer. We then calculated density of RPE cell nuclei/mm of RPE layer and the density of cells in subretinal space/mm of RPE layer. The size of RPE layer was measured from apical to basal surface of RPE. These parameters represent the loss, proliferation, and atrophy of RPE.[26]

An arbitrary scale was used to score the loss of choroidal vessels as follows: 0 indicates choroidal capillaries have good visible lumen with no intercapillary pillars; 1 indicates choroidal capillaries have good visible lumen with choroidal capillaries occupying more than 3/4 of Bruch's membrane; 2 indicates choroidal capillaries have reduced vascular lumen with choroidal capillaries occupying approximately half of Bruch's membrane; 3 indicates choroidal capillaries have reduced vascular lumen with choroidal capillaries occupying approximately 1/4 of Bruch's membrane; 4 indicates completely obliterated or absent capillaries, no lumen is visible.

Thickness of the Bruch's membrane was assessed between intercapillary pillars using electron microscopy images. Thickness of Bruch's membrane was defined as the distance between RPE side of the inner collagenous zone and the choriocapillaris side of the outer collagenous zone. Three measurements were performed for each image (the middle, left, and right part of the image).

Rabbit RBC Hemolysis Assay for Detection of Serum AP Activity

A standard rabbit red blood cell (RBC) hemolysis assay was used to measure AP activity of mouse serum. Rabbit blood (1×) (Colorado Serum Company, Denver, CO) was placed in AP buffer (GVB^{2+} with 20 mmol/L $MgCl_2$ and 8 mmol/L EGTA). After centrifugation, pellet was resuspended in the AP buffer and aliquots of 20% serum from WT, $Cd46^{-/-}$, and $Cfb^{-/-}$ mice added as described.[33] After a 2-hour incubation at 37°C, hemolysis was measured at an OD of 405 nm. Lysis of rabbit RBCs in water served as the positive control, whereas rabbit RBCs in AP buffer served as the negative control. Hemolysis was determined by an OD ratio of the following: (20% serum with RBC in AP buffer − 20% serum without RBC in AP buffer)/(RBC in water − RBC in AP buffer).

Western Blot Analysis

Fresh serum from 2-month-old male WT, $Cd46^{-/-}$, $C3^{-/-}$, $Cfb^{-/-}$, and $Cfp^{-/-}$ mice ($n = 3$ mice per group) was used to measure C3, FB, and P by Western blot. To measure rhodopsin and vascular endothelial growth factor (VEGF), retina-RPE-choroid tissue pooled separately from 2-month-old male WT and $Cd46^{-/-}$ mice and from 12-month-old male WT and $Cd46^{-/-}$ mice ($n = 4$ mice per group) was used. Reduced samples were subjected to 10% SDS-PAGE and then transferred to nitrocellulose. Goat anti-mouse C3 (MP Biomedicals), goat anti-human FB (Complement Technology), rabbit anti-mouse properdin,[36] sheep anti-rhodopsin (Abcam, Cambridge, MA), rabbit anti-VEGF (Abcam), and mouse anti−β-actin (Sigma) Abs were incubated with the membranes for 2 hours at room temperature or overnight. Secondary horseradish peroxidase−conjugated rabbit anti-goat IgG (Sigma-Aldrich), donkey anti-rabbit IgG (GE Healthcare UK Limited), goat anti-rabbit IgG, donkey anti-sheep IgG, or goat anti-mouse IgG (all from Santa Cruz Biotechnology, Dallas, TX) were added for 1 hour at 37°C. Membranes were developed with a Super-Signal West Kit (Pierce). Quantification of protein bands was accomplished by analyzing the intensity of the bands using ImageJ.

Statistical Analysis

Sample size was determined statistically before starting the experiment. Animals were numbered and selected for experiment using simple randomization by masked selection of an animal number. Damaged eyes were excluded from the analysis. All available samples ($n = 4$ to 14 mice per group) were used. Multiple measurements (at least three) for each parameter were performed independently by three investigators in a masked manner. Mean value for these parameters was calculated for each mouse. Statistical analysis was performed using Statistica program (StatSoft, Inc., Tulsa, OK). Data were analyzed and compared using one-way analysis of variance, followed by Newman-Keuls post hoc test, and differences were considered statistically significant at $P < 0.05$. Data are presented as mean value (M) ± SEM. We analyzed the effect of genotype (WT versus $Cd46^{-/-}$), the effect of age (2 versus 12 months), and the effect of sex (male versus female) for all parameters investigated. P values are shown in Supplemental Tables S1−S13.

Results

Systemic and Local (Ocular) Complement Activation in $Cd46^{-/-}$ Mouse

First, we determined the status of the AP in 2-month-old mice. Western blotting was used to assess C3, factor B, and P serum antigenic levels in WT, $Cd46^{-/-}$, $C3^{-/-}$, $Cfb^{-/-}$, and $Cfp^{-/-}$ mice (Figure 1A). AP functional activity of $Cd46^{-/-}$ mouse serum was also assessed using a rabbit RBC hemolysis assay (Figure 1B). Serum samples from WT and FB knockout mice were used as positive and negative controls, respectively. There was a normal antigen level of serum C3, FB, and P in $Cd46^{-/-}$ mouse, indicating that there was not excessive systemic turnover of the AP; likewise, functional activity was also equivalent between WT and $Cd46^{-/-}$ mice (Figure 1, A and B, and Supplemental Table S1). We next performed Western blotting only to

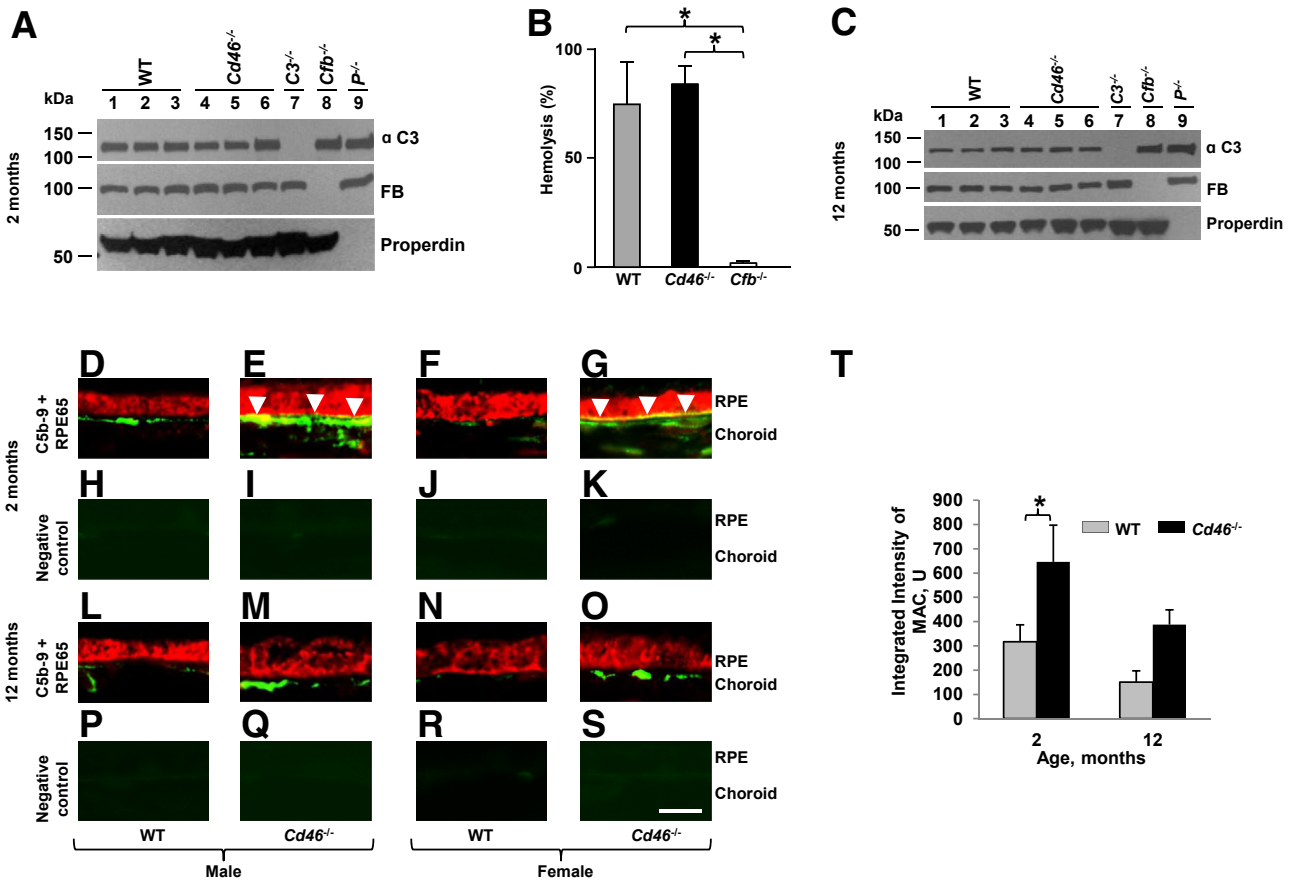

Figure 1 Systemic and ocular complement activation in *CD46*$^{-/-}$ mouse. Western blots of serum alternative pathway (AP) components in *Cd46*$^{-/-}$ and control mice at 2 (**A**) and 12 (**C**) months of age. **B:** Measurement of AP activity in sera derived from 2-month-old wild type (WT), *Cd46*$^{-/-}$, *P*$^{-/-}$, and *Cfb*$^{-/-}$ mice using a rabbit red blood cell (RBC) hemolysis assay. One-way analysis of variance was used. *Cd46*$^{-/-}$ mouse maintains a normal level of AP activity in the serum at 2 (**A** and **B**) and 12 (**C**) months of age. **D**—**S:** Representative confocal photomicrographs of paraffin sections of retinal pigment epithelium (RPE) and choroid stained for complement activation product, MAC (C5b-9). Green denotes MAC staining and red staining for RPE65, a RPE cell marker. **H**—**K** and **P**—**S:** Negative control sections show extremely low levels of autofluorescence. Localization of MAC is observed on the choroid in male and female WT and *Cd46*$^{-/-}$ mice at 2 (**D**—**G**) and 12 (**L**—**O**) months of age. Increased C5b-9 positive signal is observed in the RPE-choroid of both male and female *Cd46*$^{-/-}$ mice at 2 and 12 months of age compared with age-matched WT mice at these time points. However, in RPE cells MAC deposition (yellow when red and green merge; **arrowheads**) is statistically significant only in 2-month-old *Cd46*$^{-/-}$ male (**E**) and female (**G**) mice. **T:** Integrated intensity of MAC positive fluorescence measured using ImageJ. Statistically significant increase in MAC staining is noted in the RPE-choroid of 2-month-old *Cd46*$^{-/-}$ mouse compared with 2-month WT control. Error bars represent means ± SEM (**B** and **T**). $n = 3$ mice per group (**A** and **C**); $n = 4$ mice per group (**B**); $n = 6$ mice per group (**D**—**T**). $^*P < 0.05$ (one way analysis of variance). Scale bar = 10 μm (**D**—**S**). Original magnification, ×63 (**D**—**S**). FB, factor B; U, units.

assess C3, factor B, and properdin serum levels in WT, *Cd46*$^{-/-}$, *C3*$^{-/-}$, *Cfb*$^{-/-}$ and *Cfp*$^{-/-}$ mice at 12 months of age. Again, we obtained no evidence to suggest increased AP activation in the circulation of 12-month-old *Cd46*$^{-/-}$ mice as well (Figure 1C).

The presence of the MAC is strong evidence of complement activation,[1,27,30] and was used as a marker of such in the eye. IF using polyclonal anti-mouse C9 Ab was used to localize MAC in the RPE and choroid of 2- and 12-month-old *Cd46*$^{-/-}$ and WT mice. Polyclonal anti-mouse C9 Ab recognizes a neoepitope in C9 that arises when C9 is a part of the MAC. MAC staining (green color) was detected in the choroid of both male and female WT mice and *Cd46*$^{-/-}$ mice at the age of 2 (Figure 1, D—G) and 12 months (Figure 1, L—O). Consistent with our previous report,[28] increased MAC deposition was observed on the RPE-choroid of both male and female *Cd46*$^{-/-}$ mice compared with their WT controls at both time points. MAC deposition (Figure 1, E and G) was noted on the basal surface of RPE65 positive (Figure 1) RPE cells as a granular staining in 2-month-old male and female *Cd46*$^{-/-}$ mice. Control samples in which equal concentration of normal rabbit serum was substituted for the primary Ab showed no positive signal (Figure 1, H—K and P—S). Figure 1T summarizes the results. Statistically significant ($P < 0.05$) increase in MAC deposition was observed on the RPE-choroid of 2-month-old *Cd46*$^{-/-}$ mice compared with their WT control (Supplemental Table S2).

Together, these results demonstrate that *Cd46*$^{-/-}$ mice have normal AP activating ability in the serum, but the absence of ocular CD46 leads to dysregulated complement activation in the eye.

To Assess the *Cd46*$^{-/-}$ Mouse as a Model for Dry AMD

We analyzed and compared ocular tissue (retina, RPE, and choroid) from male and female *Cd46*$^{-/-}$ and WT mice at 2 (adult) and 12 months (aged) relative to the development of the following cardinal signs of dry AMD.

RPE Autofluorescence

RPE autofluorescence was examined because clinical studies have shown that age-dependent accumulation of lipofuscin granules and the resulting excess autofluorescence are associated with RPE atrophy, a key pathologic event of human dry AMD.[2,3,6] To detect RPE autofluorescence, thick (3 μm thick) optical slices of paraffin sections from 2- and 12-month-old *Cd46*$^{-/-}$ and WT mice were used using confocal microscopy to obtain a strong signal for analysis. Granules of autofluorescent material were occasionally detected in RPE of 2-month-old male and female *Cd46*$^{-/-}$ and WT mice (Figure 2, A–D). RPE autofluorescence in 2-month-old mice was not affected by the sex or genotype (Figure 2I and Supplemental Table S3). In WT 12-month old mice of both sexes, autofluorescence was higher (Figure 2, E and G) compared with 2-month-old WT controls (Figure 2, A and C). However, these differences were not statistically significant (Figure 2I and Supplemental Table S3). In contrast, a dramatic increase ($P < 0.05$) in RPE autofluorescence was observed in 12-month-old male and female *Cd46*$^{-/-}$ mice (Figure 2, F, H, and I and Supplemental Table S3) compared with age and genotype matched controls (Figure 2, E, G and I and Supplemental Table S3).

BM

Because there is a relationship between condition of BM and AMD,[2–4,6,9] electron microscopy was used to examine BM in male and female *Cd46*$^{-/-}$ and WT mice at 2 and 12 months of age. In male and female WT mice, the appearance of the BM was similar at 2 to that at 12 months (Figure 3, A, C, E and G). In 2-month-old *Cd46*$^{-/-}$ mice (Figure 3, B and D), the morphology of the BM was not different from that observed in WT mice (Figure 3, A and C) at the same time point. In 12-month-old male and female *Cd46*$^{-/-}$ mice, the BM was irregular with local deposition of electron dense material. This resulted in increased thickness of BM in 12-month-old male and female *Cd46*$^{-/-}$ mice (Figure 3, F, H and I) compared with 2-month-old *Cd46*$^{-/-}$ mice (Figure 3, B, D and I) and age-matched WT controls (Figure 3, E, G and I). These differences were statistically significant (Figure 3I and Supplemental Table S4).

Morphological Investigation

Age-related changes in *Cd46*$^{-/-}$ male and female mice were assessed by examining the morphology of the retina, RPE, and choroid using plastic sections (1 μm thick) stained with Toluidine Blue and Basic Fuchsin.

Retina

Loss of photoreceptors is a key feature of retinal degeneration associated with dry AMD.[2,6] ONL, POS, and PIS were examined for signs of cell death. No apoptotic bodies were detected in ONL of WT animals (Figure 4, A, C, E, and G). We found few apoptotic bodies (one to two per 10 sections) in ONL of 2-month-old *Cd46*$^{-/-}$ mice (Figure 4B) but

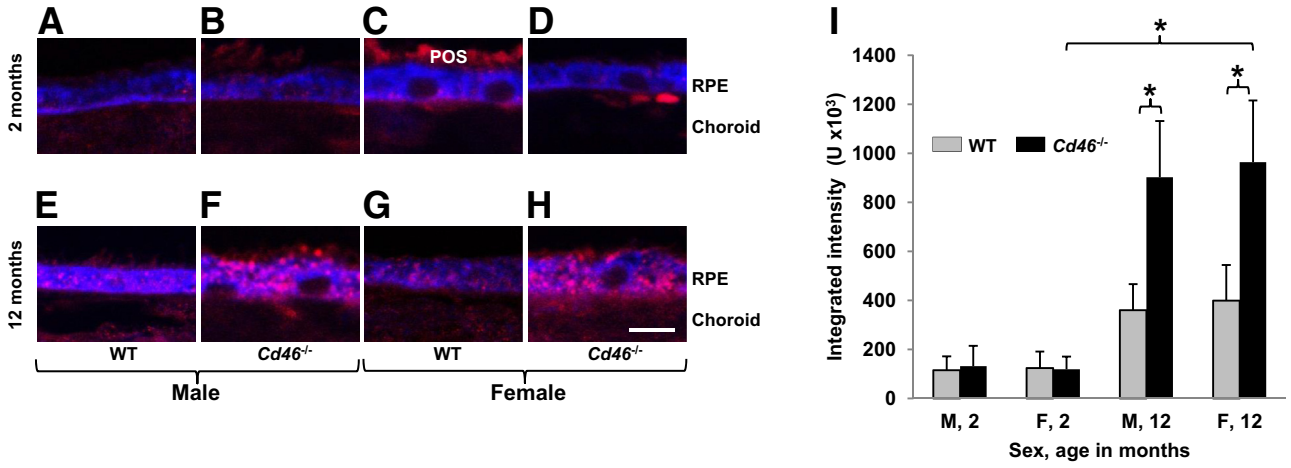

Figure 2 Retinal pigment epithelium (RPE) autofluorescence in *Cd46*$^{-/-}$ mouse. Integrated intensity of autofluorescence (red color) in RPE65 positive RPE (blue color) was measured with ImageJ. Integrated intensity of fluorescence is obtained by summation of intensity (from 0 to 255 for eight-bit image) of all pixels within defined region (RPE65-positive RPE cells). Representative confocal photomicrographs show that 2-month-old wild-type (WT) male (**A**), WT female (**C**), *Cd46*$^{-/-}$ male (**B**), and *Cd46*$^{-/-}$ female (**D**) mice have rare autofluorescent granules (red color) in RPE cytoplasm. More autofluorescent granules are seen in 12-month-old male (**E**) and female (**G**) WT mice compared with 2-month-old sex-matched WT animals (**A** and **C**), but the differences are not statistically significant (**I**). Significantly increased autofluorescence is detected in RPE of 12-month-old male (**F** and **I**) and female (**H** and **I**) *Cd46*$^{-/-}$ mice compared with age- and sex-matched WT mice at this time point (**E**, **G**, and **I**), as well as sex-matched *Cd46*$^{-/-}$ mice at 2 months of age (**D** and **I**). Paraffin sections of the eyes were not treated with Sudan Black. In these experiments, autofluorescence in the choroid and POS was not measured. Error bars represent means ± SEM (**I**). $n = 5$ mice per group (**I**). *$P < 0.05$ (one-way analysis of variance). Scale bar = 10 μm (**A**–**H**). Original magnification, ×63 (**A**–**H**). F, female; M, male; POS, photoreceptor outer segment.

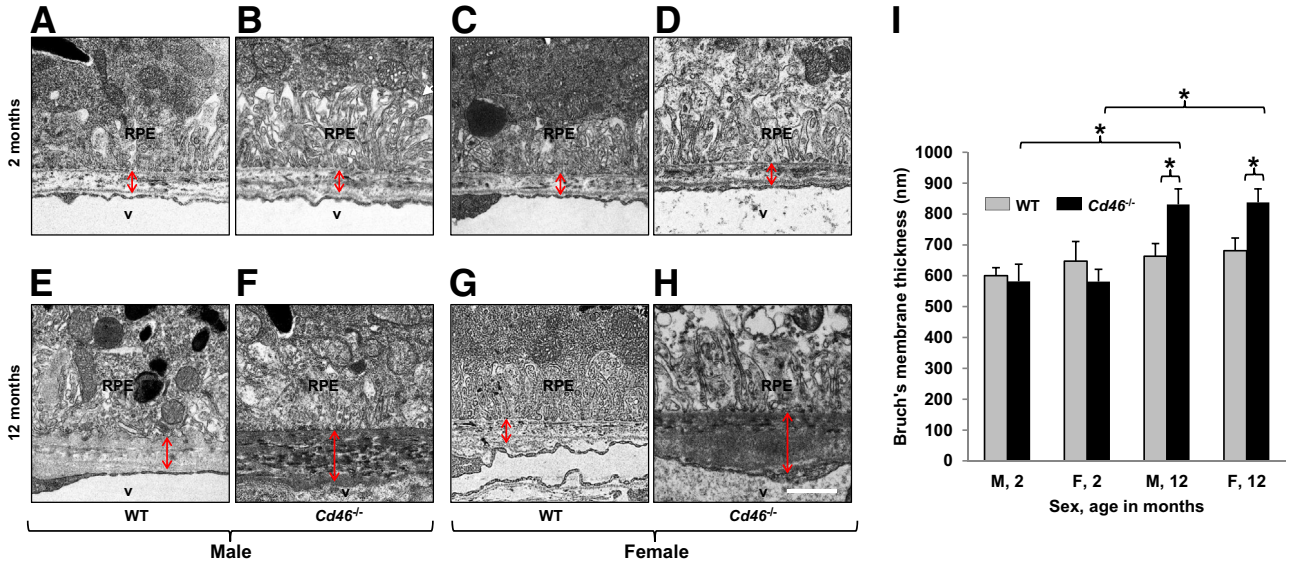

Figure 3 Age-related changes in Bruch's membrane (BM) thickness in *Cd46*$^{-/-}$ mouse. Thin plastic sections were analyzed using electron microscopy. Representative electron micrographs of the eyes harvested from 2- and 12-month-old male and female wild-type (WT) (**A**, **C**, **E**, and **G**) and *Cd46*$^{-/-}$ (**B**, **D**, **F**, and **H**) mice. Thickness of BM was measured (**arrows**). There is no difference in the thickness of BM between 2-month-old WT male (**A**) and *Cd46*$^{-/-}$ male (**B**) as well as WT female mice (**C**) and *Cd46*$^{-/-}$ female (**D**) mice. **E**, **G**, and **I:** BM thickness does not change in 12-month-old male and female WT mice. **F**, **H**, and **I:** In contrast, local accumulation of dense deposits and increased thickness of BM is observed in 12-month-old male and female *Cd46*$^{-/-}$ mice. Error bars represent means ± SEM (**I**). $n = 5$ to 9 mice per group (**I**). *$P < 0.05$ (one-way analysis of variance). Scale bar = 1 μm (**A**–**H**). Original magnification, ×5000 (**A**–**H**). F, female; M, male; RPE, retinal pigment epithelium; v, lumen of choroidal vessels.

many more apoptotic bodies (one to three per section) in 12-month-old *Cd46*$^{-/-}$ mice (Figure 4F). In *Cd46*$^{-/-}$ mice, shortening of the inner portion of the photoreceptor was only observed close to apoptotic bodies in ONL (Figure 4F), but the average thickness of PIS and POS were not affected (Figure 4J and Supplemental Table S5).

We did not observe any significant changes in thickness of ONL among investigated groups (Figure 4, A–I and Supplemental Table S6). However, the density of nuclei in ONL was significantly ($P < 0.05$) reduced in 12-month-old *Cd46*$^{-/-}$ mice (male and female) (Figure 4, F, H, and K and Supplemental Table S7) compared with age-matched WT controls (Figure 4, E and G and Supplemental Table S7). Similar results were obtained when 12-month-old *Cd46*$^{-/-}$ mice were compared with 2-month-old *Cd46*$^{-/-}$ mice (Figure 4, B, D, and K and Supplemental Table S7).

Western blot analysis for rhodopsin protein was next performed to determine whether the number of photoreceptors was reduced in *Cd46*$^{-/-}$ mouse. Rhodopsin, a member of the G-protein–coupled receptor family, is located in photoreceptor cells of the retina and a decline in rhodopsin content is observed with progression of AMD in humans.[37] Rhodopsin blot detected isoforms between 40 and 160 kDa in WT and *Cd46*$^{-/-}$ mouse at 2 and 12 months of age (Figure 5A). Densitometric analysis revealed a statistically significant reduction of total rhodopsin protein in *Cd46*$^{-/-}$ mice at 12 months of age compared with that at 2 months when normalized to WT controls at both time points (Figure 5B and Supplemental Table S8). Finally, we observed that all 12-month-old *Cd46*$^{-/-}$ mice (males and females) had reduced density of nuclei in ONL (Figure 5, C and D and Supplemental Table S7).

RPE and Choroid

Histological analysis revealed that the appearance of RPE, Bruch's membrane, and choroidal capillaries was similar in all WT samples (Figure 6, A, C, E, and G). In 2-month-old *Cd46*$^{-/-}$ mice, we occasionally found RPE cells with dark cytoplasm and condensed nuclei (Figure 6B). The number of RPE cells was not significantly different between *Cd46*$^{-/-}$ and WT mice at 2 and 12 months of age (Figure 6I and Supplemental Table S9). However, the size of RPE layer measured from apical to basal surface significantly ($P < 0.05$) increased in 12-month-old *Cd46*$^{-/-}$ male and female mice (Figure 6, F, H, and J and Supplemental Table S10) compared with age-matched controls (Figure 6, E, G, and J and Supplemental Table S10). We observed macrophage-like cells containing different amounts of pigment located in the subretinal space in all groups (Figure 6, D, F, and K), except 2-month-old WT males. These cells located in subretinal space were positive for marker RPE65 (data not shown). Interestingly, the number of macrophage-like cells in the subretinal space significantly ($P < 0.05$) increased in 12-month-old male and female *Cd46*$^{-/-}$ mice (Figure 6K and Supplemental Table S11). We observed accumulation of dense amorphous material (stained pink with Toluidine Blue and Basic Fuchsin) on semithin sections. These basophilic deposits were present between RPE and choriocapillaries (Figure 6H) only in 12-month-old *Cd46*$^{-/-}$ mice. Zones of hypercellularity were

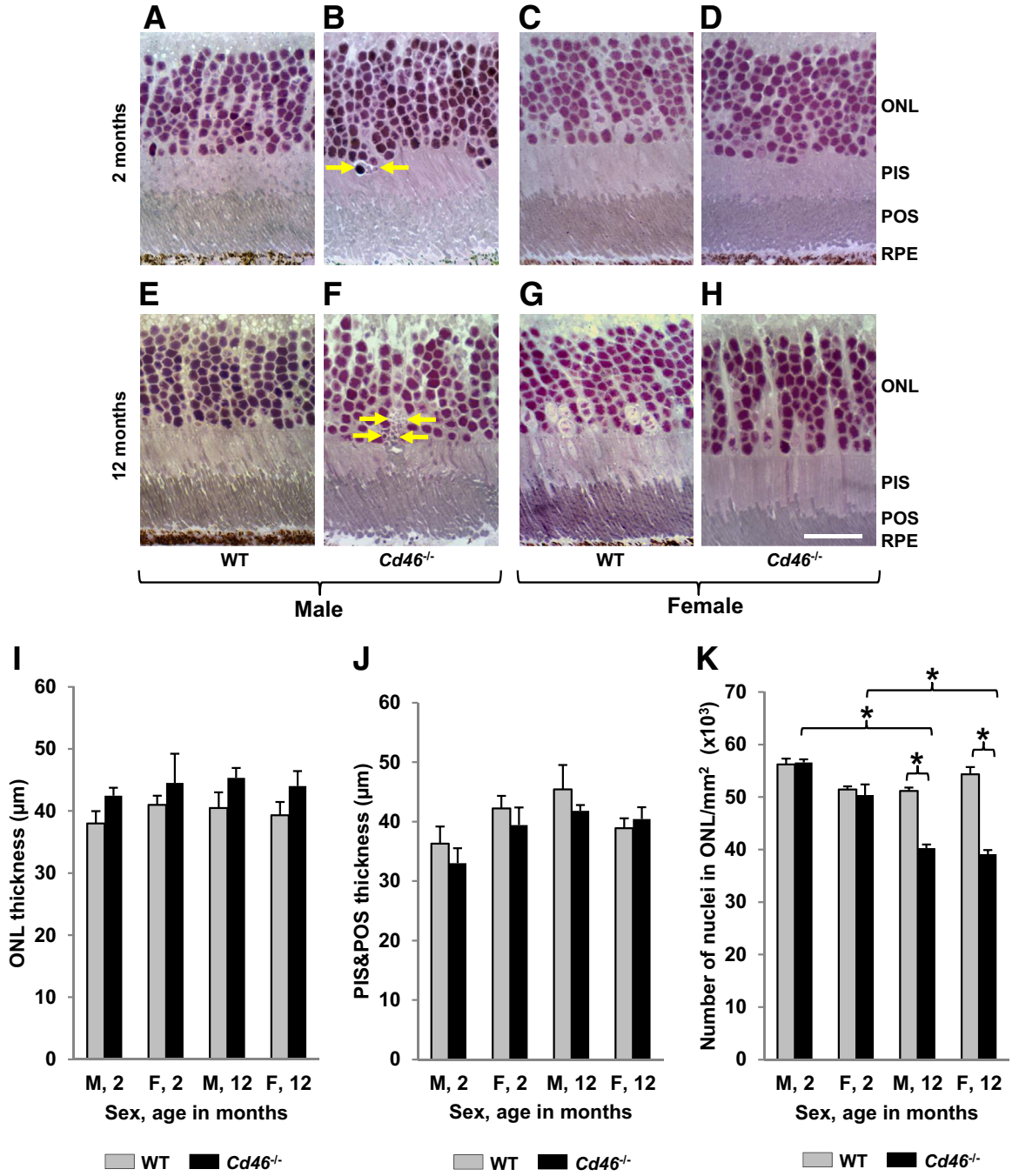

Figure 4 Degenerative changes in photoreceptors in *Cd46*$^{-/-}$ mouse. Plastic sections (1 µm thick) of posterior part of mouse eye were stained with Basic Fuchsin and Toluidine Blue, and images of the sections were captured. Thickness of photoreceptor layer was measured using ImageJ. Representative images from WT (**A**, **C**, **E**, and **G**) and *Cd46*$^{-/-}$ (**B**, **D**, **F**, and **H**) mice. Few apoptotic bodies are detected in outer nuclear layer (ONL) of 2-month-old *Cd46*$^{-/-}$ male (**B**, **arrows**) mice, but several apoptotic bodies are detected in male *Cd46*$^{-/-}$ mice at 12 months of age (**F**, **arrows**). **A**–**H**, **I**, and **J:** ONL thickness and combined photoreceptor inner segment (PIS) and photoreceptor outer segment (POS) lengths are similar among all investigated groups. However, the number of nuclei in ONL is significantly reduced in 12-month-old *Cd46*$^{-/-}$ male and female mice (**F**, **H**, and **K**) compared with age-matched wild-type (WT) controls (**E**, **G**, and **K**) and 2-month-old *Cd46*$^{-/-}$ mice (**B**, **D**, and **K**). Error bars represent means ± SEM (**I**–**K**). $n = 6$ to 9 mice per group (**I**–**K**). *$P < 0.05$ (one-way analysis of variance). Scale bar = 20 µm (**A**–**H**). Original magnification, ×40 (**A**–**H**). F, female; M, male; RPE, retinal pigment epithelium.

noted in the choroid of 12-month-old *Cd46*$^{-/-}$ mice (Figure 6H).

The presence of vacuoles in cytoplasm is a sign of RPE degeneration.[38–41] In WT male and female mice, none or only a few vacuoles in the cytoplasm of RPE cells were detected at 2 and 12 months of age (Figure 6, A, C, E, and G). We observed an increased number of vacuoles in RPE cytoplasm of *Cd46*$^{-/-}$ mice (Figure 6, B, D, F, and H)

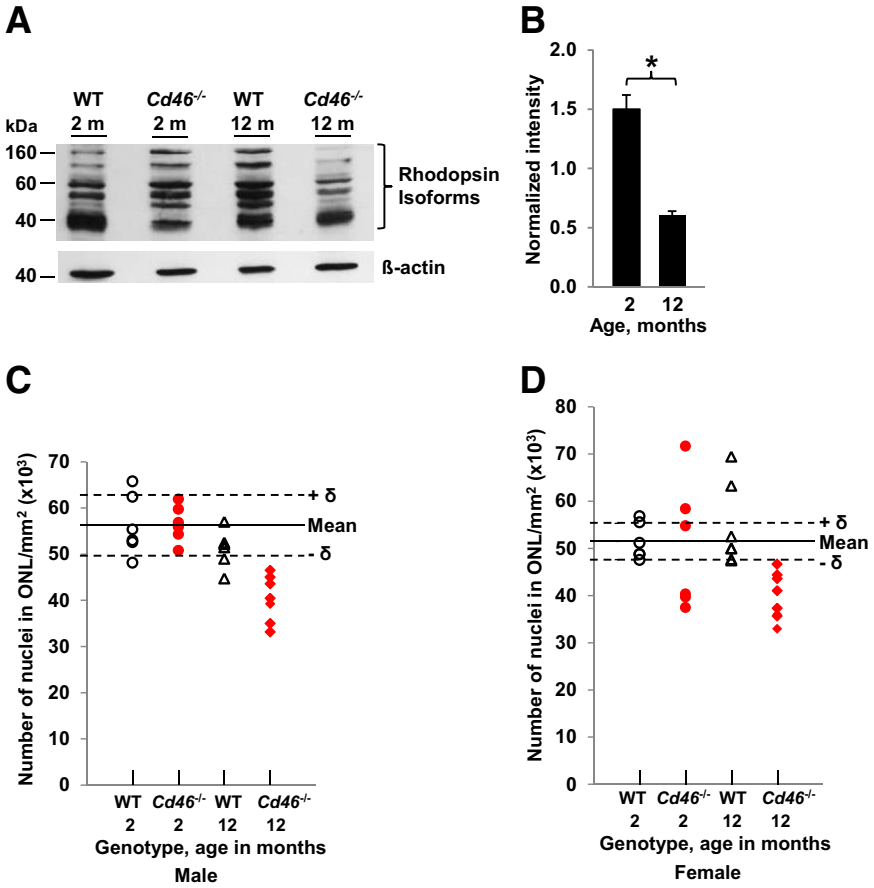

Figure 5 **A:** Rhodopsin isoform levels in $CD46^{-/-}$ mouse. Representative Western blot shows rhodopsin isoforms (40 to 160 kDa) in the retina and the choroid of wild-type (WT) and $Cd46^{-/-}$ animals at 2 and 12 months of age. β-actin was used as loading control and blots for rhodopsin and β-actin were performed separately. **B:** Density of all rhodopsin isoforms (40 to 160 kDa) was measured on rhodopsin blot and density of β-actin band was measured on β-actin blot. For each sample, the intensity of rhodopsin isoforms was normalized to the intensity of β-actin protein band. The densitometric analysis of blots is expressed as the ratio of the intensity of the rhodopsin isoforms in $CD46^{-/-}$ mouse at 2 and 12 months of age to the intensity of rhodopsin isoforms in WT at 2 and 12 months of age, respectively. Statistically significant reduction of total rhodopsin content in retina and retinal pigment epithelium (RPE)-choroid is observed in 12-month-old $Cd46^{-/-}$ mice compared with 2-month-old $Cd46^{-/-}$ mice. Reduction of outer nuclear layer (ONL) nuclei density is noted in all male (**C**) and female (**D**) 12-month-old $Cd46^{-/-}$ mice more than 1 δ (SD, **dashed line**) compared with mean (**solid line**) found in 2-month-old WT mice. Data presented as means ± SEM (**B**). $n = 4$ mice per group (**B**). $^{*}P < 0.05$ (one-way analysis of variance).

compared with age and sex-matched WT controls. Autophagy is activated in response to aging. This results in the accumulation of waste material (cellular debris) within resident ocular cells.[42] RPE cells were examined to detect the sign of autophagy: waste material by light microscopy and autophagosome by electron microscopy. In WT mice, no cellular debris was detected in RPE cells when epon sections were examined under light microscope (Figure 7A). In contrast, some RPE cells containing cellular debris were detected in $Cd46^{-/-}$ mice (Figure 7B). Examination of epon sections under the electron microscope revealed the absence of such cellular debris in WT mice (Figure 7C). However, vesicles and double layered structures (autophagosomes) containing cellular organelles (mitochondria, lipofuscin, and pigmented granules) were detected in $Cd46^{-/-}$ mice by electron microscopy (Figure 7, D–G).

Examination of Choroidal Capillaries

Choroid capillaries were examined by light and electron microscopy. WT mice showed normal structure of the choriocapillaries (Figure 7, A and C). However, the lumen of choroidal capillaries was reduced in $Cd46^{-/-}$ mice (Figure 7, B and D). When examined by electron microscopy, some choroidal endothelial cells in $Cd46^{-/-}$ mice had no lumen or cytoplasmic fenestrae at 12 months (Figure 7D). Statistically significant reduction ($P < 0.05$) of the choroidal vasculature was found in 12-month-old $Cd46^{-/-}$ male and female mice, and this reduction was age dependent (Figure 7H and Supplemental Table S12).

Angiography of Choroidal Vasculature

We performed angiography of choroidal vessels in 2- and 12-month-old male animals using laser confocal microscopy and built three-dimensional models of choroidal vessels (Figure 8, A–D). Intense green fluorescence was observed in the choroidal vessels perfused with FITC-dextran. FITC-dextran perfused vessels occupied almost the entire area of the choroid in 2- and 12-month-old WT mice and 2-month-old $Cd46^{-/-}$ mice. We observed increased space (dark zones) between FITC-perfused choroidal vessels in 12-month-old $Cd46^{-/-}$ mice. The density of choroidal vessels was measured as the percentage (%) of green fluorescence (FITC-dextran) on the entire image. Results in Figure 8 demonstrate that the choroidal vessels were located close to each other in 2-month-old WT and $Cd46^{-/-}$ mice (Figure 8, A and B). However, at 12 months, the density of the choroidal vessels was significantly ($P < 0.05$) reduced in $Cd46^{-/-}$ mice (Figure 8, D and E and Supplemental Table S13) compared with WT animals (Figure 8, C and E and Supplemental Table S13).

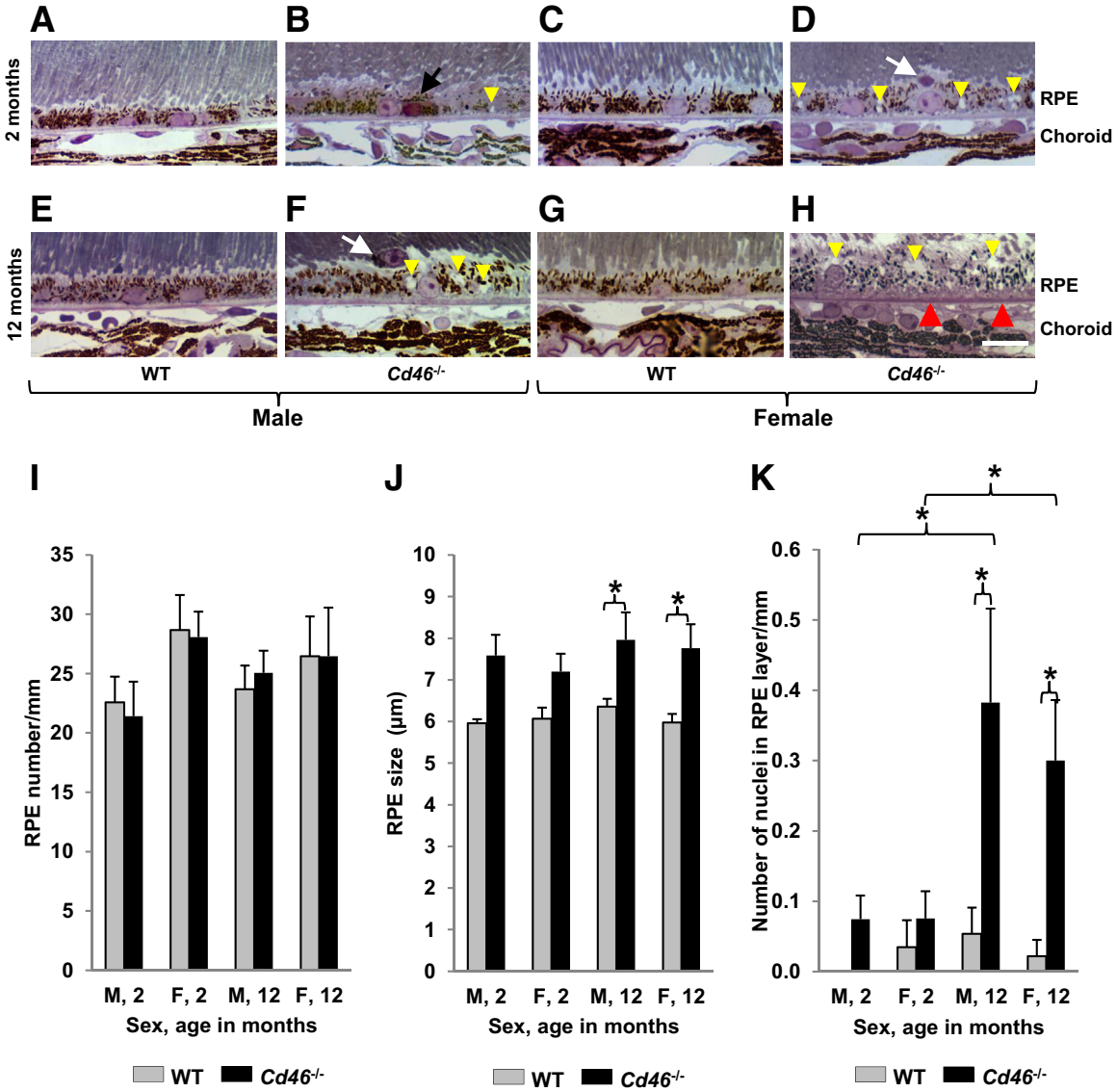

Figure 6 Age-dependent degenerative changes in retinal pigment epithelium (RPE) and choroid of *Cd46*$^{-/-}$ mouse eyes. **A**–**H:** Plastic sections (1 μm thick) of eyes were stained with Basic Fuchsin and Toluidine Blue and observed under light microscope. Nuclei with condensed chromatin and shrinkage of cytoplasm in some RPE cells (**black arrow**, **B**), cells containing pigmented granules located in subretinal space (**white arrows**, **D** and **F**) are detected in *Cd46*$^{-/-}$ mice at 2 and 12 months of age. Basophilic deposits between RPE and choroid capillaries (**red arrowheads**) are detected in *Cd46*$^{-/-}$ mice at 12 months of age. The number of RPE nuclei is similar in all investigated groups (**I**), but the size of RPE layer measured from apical to basal surface of RPE is significantly increased in 12-month-old *Cd46*$^{-/-}$ mice compared with age- and sex-matched wild-type (WT) controls (**J**). **K:** The number of cells in subretinal space (calculated per mm of the RPE layer) is significantly increased in 12-month-old male and female *Cd46*$^{-/-}$ mice compared with WT controls. In *Cd46*$^{-/-}$ mice, more vacuoles are present in RPE cytoplasm (**yellow arrowheads**, **B**, **D**, **F**, and **H**). Error bars represent means ± SEM (**I**–**K**). $n = 6$ to 13 mice per group (**I**–**K**). *$P < 0.05$ (one-way analysis of variance). Scale bar = 10 μm (**A**–**H**). Original magnification, ×40 (**A**–**H**). F, female; M, male.

VEGF Levels

To further decipher the underlying mechanism responsible for reduced density of choroidal vessels in 12-month-old *Cd46*$^{-/-}$ mouse, Western blot analysis was performed to compare VEGF levels in the retina-RPE-choroid tissue from *Cd46*$^{-/-}$ and WT mice at 2 and 12 months of age. VEGF is a major growth factor responsible for the maintenance of normal choroidal vasculature.[43] We observed statistically significant reduction of VEGF isoforms (approximately 18 and 43 kDa) in 12-month-old *Cd46*$^{-/-}$ mice compared with 2-month-old *Cd46*$^{-/-}$ mice when normalized to WT controls at both time points (Figure 8, F–H and Supplemental Table S8).

In summary, as the *Cd46*$^{-/-}$ mice aged, 60% accumulated lipofuscin in the RPE, 57% had Bruch's membrane thickening, 73% had excessive number of cells in the subretinal space, 100% lost nuclei in the ONL, 58% developed an increase in RPE size, and 80% had a diminution in the choriocapillaris.

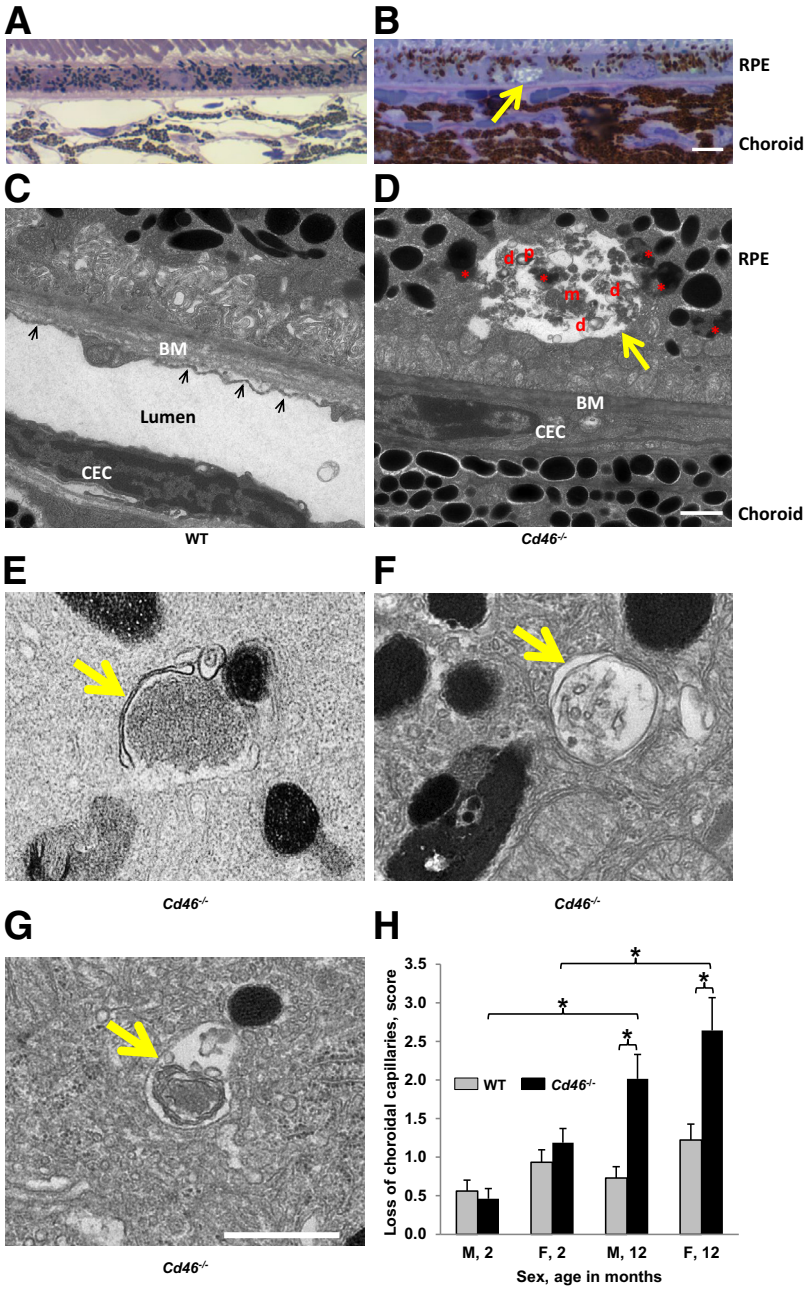

Figure 7 Pathologic changes in retinal pigment epithelium (RPE) and choroid. Epon sections of 12-month-old wild-type (WT; **A** and **C**) and *Cd46*$^{-/-}$ (**B**, **D**, and **E**–**G**) mice were examined under light (**A** and **B**) or electron (**C**–**G**) microscopy. Representative images show a vacuole (**yellow arrows** in **B** and **D**) containing partially digested cellular components: pigment granules (p), mitochondria (m), lipofuscin-like granules (**red asterisks**), and double-layered membranous structures (d) in *Cd46*$^{-/-}$ mice. **D:** Numerous lipofuscin-like granules (**red asterisks**) are found in cytoplasm of RPE in *Cd46*$^{-/-}$ mice. Double-layered membranous structures (autophagosomes) were detected in *Cd46*$^{-/-}$ mice (**yellow arrows**, **E**–**G**). **D:** In *Cd46*$^{-/-}$ mice, Bruch's membrane (BM) elastic and collagenous layers are not observed; instead, accumulation of electron dense amorphous material is seen. In 12-month-old *Cd46*$^{-/-}$ mice, choroid endothelial cells (CECs) with signs of dedifferentiation are shown. In 12-month-old *Cd46*$^{-/-}$ mice, CECs have no lumen and cytoplasmic fenestrae (**D**) as observed in WT sample (**black arrows** in **C**). **H:** Loss of choroidal vessels (shown as an arbitrary score) is seen in 12-month-old male and female *Cd46*$^{-/-}$ mice compared with 2-month-old male and female *Cd46*$^{-/-}$ mice and age-matched WT controls. Error bars represent means ± SEM (**H**). $n = 6$ to 13 mice per group (**A**–**G**); $n = 6$ to 9 mice per group (**H**). $^{*}P < 0.05$ (one-way analysis of variance). Scale bar = 1 μm (**A**–**G**). Original magnifications: ×100 (**A** and **B**); ×5000 (**C**–**G**). F, female; M, male.

Discussion

Dry type AMD is characterized by loss of photoreceptors, a localized increase in thickness of Bruch's membrane, drusen deposits, RPE cell atrophy, and choroidal capillary alterations.[2,3,6] The management of patients with dry AMD remains a significant challenge because dry AMD is managed using non-specific therapies.[11,12] Unfortunately, these therapeutic modalities do not address the underlying primary mechanisms of disease development. Because of the lack of effective therapeutic options available to the patients with dry AMD, there is a pressing need to develop additional treatments. Animal models have played a crucial role to our understanding of AMD pathology.[18–28,38,44–77] They have provided tools necessary to understand the etiopathogenesis of this disease and have proved to be critical for preclinical studies testing new therapeutic agents.

A wealth of data suggests that overactivation of the alternative pathway (AP) of the complement system is a critical player in the pathogenesis of human AMD and its animal models.[15,16] In addition, complement activation fragments and regulators are deposited in the retina.[73,74] Genome-wide association studies have indicated that a common polymorphic variant of complement regulator factor H (FH) increases the susceptibility to AMD in humans.[75] Also, rare variants in FH are associated with AMD and have been observed in familial AMD.[76–78] Furthermore, multiple studies have also implicated

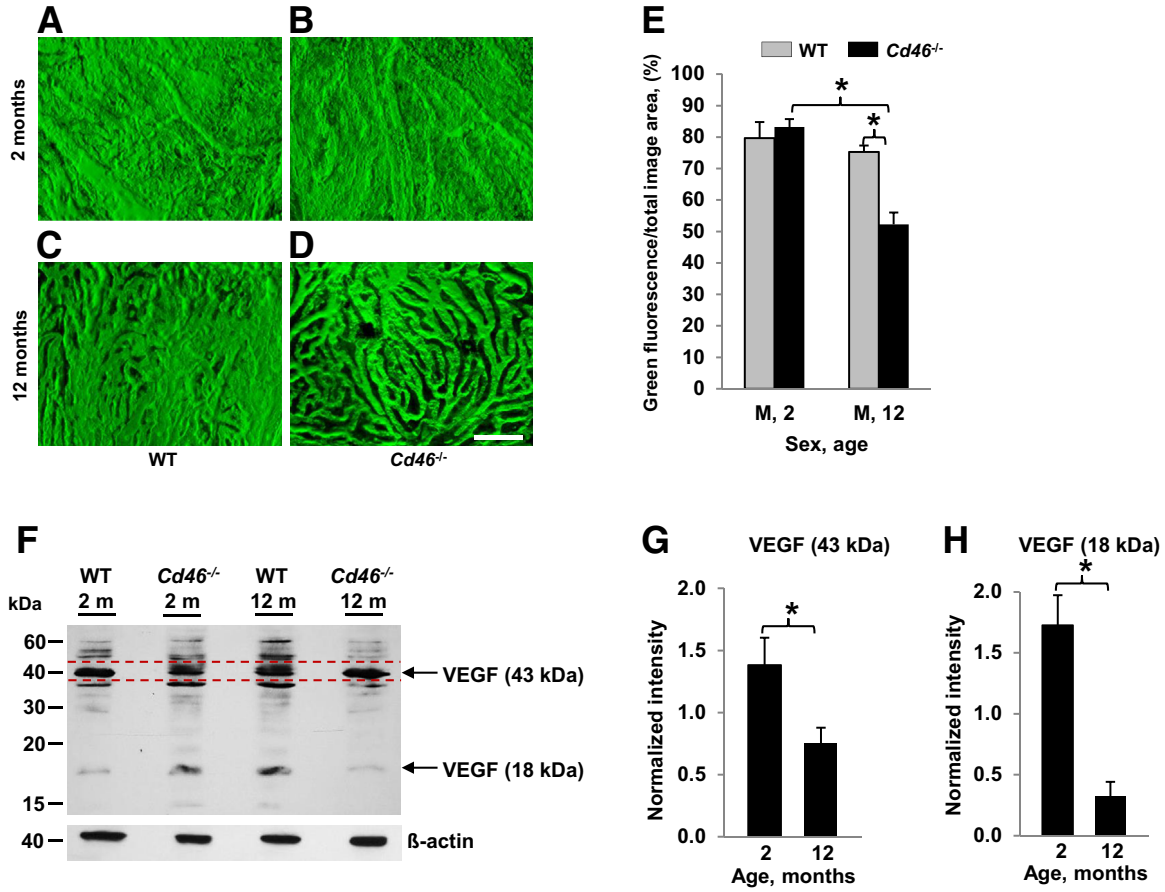

Figure 8 Loss of choroidal capillaries in the *Cd46*$^{-/-}$ mouse. Angiography of choroidal vessels was performed in male wild-type (WT) and *Cd46*$^{-/-}$ mice at 2 (**A** and **B**) and 12 (**C** and **D**) months of age. Animals were perfused with high-molecular-weight fluorescein isothiocyanate (FITC)-dextran. Retinal pigment epithelium (RPE) was removed, and images of flat-mounted choroid were captured using a laser confocal microscope. **A**—**D:** Z-stack images were used to construct a three-dimensional model of choroidal vessels. Area of FITC-dextran—perfused choroidal vessels (green) in relation to the total image area was measured using ImageJ. **E:** At the age of 12 months, the area of FITC-dextran perfused choroidal vessels (green) is significantly reduced in male *Cd46*$^{-/-}$ mice compared with sex-matched WT animals. Levels of vascular endothelial growth factor (VEGF) protein in *CD46*$^{-/-}$ mouse. **F:** Representative Western blot for VEGF using total protein isolated from pooled retina-RPE-choroid. Under reducing conditions, two protein bands are predominantly detected with an apparent molecular mass of 43 and 18 kDa. β-Actin was used as loading control and blots for VEGF and β-actin were performed separately. **G** and **H:** Density of 43- and 18-kDa bands was separately measured on VEGF blots. **F:** The band in the 43-kDa region used for quantification is marked with **red dotted lines**. Density of β-actin band was measured on β-actin blots. First, for each sample (*CD46*$^{-/-}$ or WT), the intensity of the 43- and 18-kDa VEGF bands was normalized to that of the β-actin band. Next, the intensity of VEGF band in WT animals was taken as 1. The densitometric analysis of blots is expressed as the ratio of the intensity of 43 kDa (**G**) and 18 kDa (**H**) VEGF bands in *CD46*$^{-/-}$ mouse at 2 and 12 months of age to the intensity of 43- and 18-kDa VEGF bands in WT animals at 2 and 12 months of age, respectively (**G** and **H**). The intensity of VEGF band in WT group for graphs **G** and **H** is 1. Levels of both the 43- and 18-kDa VEGF protein bands, as determined by Western blotting, are significantly reduced in the neuronal retina, RPE, and choroid harvested from the eyes of 12-month-old *Cd46*$^{-/-}$ mice compared with 2-month-old *Cd46*$^{-/-}$ mice. Error bars represent means ± SEM (**E**). $n = 6$ to 8 mice per group (**E**); $n = 4$ mice per group (**G** and **H**). *$P < 0.05$ (one-way analysis of variance). Scale bar = 100 μm (**A**—**D**). M, male.

common and rare variants in the complement proteins C3, factor B, and especially factor I in modulating the risk of AMD.[17,79]

FH is the major plasma regulatory protein of the AP; its cellular (membrane) counterpart in nonrodent primates is CD46.[29–32] CD46 is expressed nearly ubiquitously in humans.[31,32] In the mouse, CD46 was previously thought to be only expressed on the inner acrosomal membrane of spermatozoa. However, we recently described that CD46 mRNA and protein are present in the neuronal retina, RPE, and choroid of the C57BL/6 mouse.[28] Herein, the eyes from male and female WT and *Cd46*$^{-/-}$ mice were analyzed at the age of 2 (adult) and 12 (aged) months. We investigated the role of complement-mediated pathophysiology in dry AMD and indicate that *Cd46*$^{-/-}$ mouse is a promising model for dry AMD.

Systemic and ocular (local) complement activation in the *Cd46*$^{-/-}$ mouse was investigated. Our results demonstrate that *Cd46*$^{-/-}$ mouse has normal AP activating ability in serum. This result indicates that deficiency of CD46 in limited (two) sites has no detectable impact on serum AP homeostasis. However, the absence of ocular CD46 leads to dysregulated local AP activation in the eye, resulting in an AMD phenotype. Surprisingly, although a trend was noted,

we did not detect an age-related increase of MAC deposition in RPE-choroid of WT or *Cd46*$^{-/-}$ mice. This may, however, relate to the presence of the inhibitors of MAC assembly, especially CD59. Together, these results are consistent in the mouse with the expression pattern of CD46 and play a key regulatory role in retinal tissue.[28,31,32]

In our experiments, the eyes from male and female *Cd46*$^{-/-}$ mice were analyzed at the age of 2 (adult) and 12 (aged) months for age-related histological changes. We observed that, as the *Cd46*$^{-/-}$ mice age, they spontaneously develop a phenotype that closely resembles the dry form of human AMD.

Lipofuscin accumulation is a sign of impaired intracellular digestion of waste material and aging. RPE cells in human dry AMD contain elevated quantities of the autofluorescent material lipofuscin.[80,81] We detected significantly higher RPE autofluorescence in aged *Cd46*$^{-/-}$ mice. In parallel, the size of RPE was increased in these animals. Vacuolization of RPE cytoplasm is a sign of RPE degeneration and has been reported in aged mice.[38,40,45] We suggest that vacuolization may contribute to the increased RPE size observed in our present study. Electron microscopy revealed the presence of macroautophagosomes in RPE of *Cd46*$^{-/-}$ mice. Macroautophagosomes have double layered membrane and contain cytoplasm and organelles.[41,80] Their presence in a cell is a sign of autophagy. Our data suggest that autophagy may be activated in response of impaired RPE function in *Cd46*$^{-/-}$ mice, leading to the formation of macroautophagosomes. Autophagy is activated in RPE cells in response to stress and helps in the clearance of damaged cellular components.[42,82] Dysfunction of autophagy may contribute to accumulation of waste material inside the RPE (lipofuscin) and within the Bruch's membrane (drusen deposits).[11,42,73,80,83–85] The mechanism of how autophagy is initiated in *Cd46*$^{-/-}$ mice requires further study. Interestingly, no reduction in RPE nuclei number was observed in *Cd46*$^{-/-}$ mice. These results suggest that RPE cells may be relatively resistant to cell death caused by the increased complement activation or that the presence of other regulators checks the complement system's ability to perturb membranes.

Using a terminal deoxynucleotidyl transferase-mediated dUTP nick-end labeling assay and caspase 3 staining, RPE cell death was not detected in *Cd46*$^{-/-}$ mice at 2 and 12 months of age (our unpublished results). However, it is possible that in animals >12 months, cell death of RPE may be detected using these techniques.

Thickness of the BM increases with age in humans.[9,86] Risk of AMD is associated with an abnormal increase in thickness of BM as the quantity of basal laminar deposits strongly correlates with the presence of AMD.[6,86,87] In the present study, we demonstrated accumulation of dense deposits and increased thickness of BM in 12-month-old *Cd46*$^{-/-}$ mice. It is possible that in these animals the basophilic material represents dense deposits in Bruch's membrane. In previous articles, increased thickness of BM was reported in aged Ccl-2 or Ccr-2 deficient mice[57] and transgenic mice overexpressing the human biglycan and apolipoprotein b-100 genes.[70] Together, our results suggest that *Cd46*$^{-/-}$ mice generate more waste material because of excessive complement activation due to the lack of CD46. The debris accumulates within RPE cells as autofluorescent material and also is deposited in BM as dense deposits.

Loss of photoreceptors is a final irreversible event in AMD. We observed the presence of apoptotic bodies in ONL and age-related loss of photoreceptors (measured by ONL nuclei density) in all *Cd46*$^{-/-}$ mice. Photoreceptor loss started early in life (2 months) in *Cd46*$^{-/-}$ mice and continued until at least 12 months of age. Shortening of photoreceptor outer and inner segments was observed close to apoptotic bodies. We hypothesize that in *Cd46*$^{-/-}$ mice, dying photoreceptors were not able to regenerate cellular components, which led to shortening of PIS and POS. Apoptotic bodies and cellular debris moved toward RPE cells and possibly were phagocytosed by RPE cells and macrophage-like subretinal cells. The increased load of cellular material may thus contribute to accumulation of lipofuscin and dense deposits in *Cd46*$^{-/-}$ mice.

The presence of cells in the subretinal area in *Ccl2* knockout mice has been reported. The authors detected macrophages and pigment in subretinal cells and concluded that they were the source of sub-RPE deposits.[56]

We investigated choroidal vasculature using light and electron microscopy as well as FITC-dextran angiography because it is reported that reduction of choroidal vascularization may contribute to dry AMD.[2–4] Although FITC-dextran angiography is not a commonly used method to quantify choriocapillary density in naive animals, it is a well-accepted method to investigate choroidal neovascularization.[18–25] We found that at the age of 12 months the density of the choroidal vessels was significantly ($P < 0.05$) reduced in *Cd46*$^{-/-}$ mice compared with WT animals. Significantly decreased levels of VEGF in 12-month-old *Cd46*$^{-/-}$ mouse observed in our current study may lead to reduced density of choroidal vessels. However, we cannot completely rule out the possibility of dye leakage in our model. Using similar method, though, the reduction of choroidal capillaries was observed in a study using retinal dystrophic (rd)-mice.[53]

The connection of the complement system to AMD has been reported in some murine models of dry-type AMD.[25,44,51,52,54,57,62] Retinal abnormalities have been described in aged FH deficient (*Cfh*$^{-/-}$) mice.[51] However, the disease phenotype was modest because these animals displayed a partial phenotype of dry AMD. Lipofuscin accumulation in RPE cells was not accompanied by accumulation of deposits or drusen formation. Electron microscopy revealed that in *Cfh*$^{-/-}$ mice there was no loss of photoreceptors.[51] The authors suggested that apical secretion of FH is important in maintaining complement regulation in the retina of these mice. However, *Cfh*$^{-/-}$ mice have negligible AP activating capacity. In these mice, the AP is almost

completely inactive secondary to the fluid phase AP turnover.[51,88] Both FH (plasma protein) and CD46 (membrane bound protein) are regulators of the AP.[29,30] In mice, FH is ubiquitously present,[31,32] whereas CD46 is expressed only on spermatozoa[31,32] and in the eye.[28] More important, our current study shows that *Cd46*$^{-/-}$ mice have normal systemic AP-activating ability but the lack of ocular CD46 leads to dysregulated complement activation in the retina and choroid. To summarize, our data suggest that the local (ocular) but not systemic control of the AP is crucial in the pathogenesis of dry AMD.

In another study, chimeric FH proteins were expressed in *Cfh*$^{-/-}$ mice (*CfhTg/mCfh*$^{-/-}$). In the eyes of these animals, a dry AMD phenotype was more severe than in *Cfh*$^{-/-}$ mice.[49] Using enzyme-linked immunosorbent assay, the authors reported that *CfhTg/mCfh*$^{-/-}$ mouse has normal serum C3 levels, indicating a fully functional systemic AP in these animals. Chimeric mice in which the serum C3 was normal indicates that an intact AP is required to develop a more full-blown model of AMD.

In 2013, a survey of strains in the JAX Mouse Repository detected a number of founder mutations, including *Pde6b*^{rd1}and *Crb*^{rd8}among the mouse strains.[89] Because retinal pathology may occur in the presence of *Pde6b*^{rd1}or *Crb*^{rd8}mutations, genotyping was performed to determine whether *Cd46*$^{-/-}$ mice carry these mutations. Using PCR analysis, we observed that *Cd46*$^{-/-}$ mice do not carry *Pde6b*^{rd1}but carry *Crb*^{rd8} (data not shown). In contrast, WT animals do not carry the *Crb*^{rd8}mutation (data not shown). It is possible that *Crb*^{rd8}mutation detected in *Cd46*$^{-/-}$ mouse was derived from the embryonic stem cells used for the generation of these animals. Many embryonic stem cell lines used to generate genetically modified mice carry the *Crb*^{rd8}mutation.[89]

To investigate if the spontaneous age-related degenerative changes in the retina, RPE, and choroid of *Cd46*$^{-/-}$ mice observed in our study are in some way related to *Crb*^{rd8}, we analyzed ocular tissue (retina, RPE, and choroid) from *Cd46*$^{-/-}$*fB*$^{-/-}$ double knockout mice at 12 months of age. Because factor B is an integral component of the AP, its activation is abrogated in *Cd46*$^{-/-}$*fB*$^{-/-}$ mice. Our unpublished and ongoing studies indicate that *Cd46*$^{-/-}$*fB*$^{-/-}$ genotype is protective against development of the key features of dry AMD in our *Cd46*$^{-/-}$ model system. Furthermore, it has been reported that photoreceptor degeneration in mice with *Crb*^{rd8}mutation strongly varies with the genetic background.[90] Thus, on the basis of these background data and our results with *Cd46*$^{-/-}$*fB*$^{-/-}$ mice, we conclude that spontaneous age-related degenerative changes in the retina, RPE, and choroid of *Cd46*$^{-/-}$ mice are caused by the lack of ocular CD46.

Collectively, our results show that, as *Cd46*$^{-/-}$ mice age, they develop degenerative changes in the retina, RPE, and choroid. These alterations are similar to those observed in patients with the dry type of AMD. The AP's amplification loop is a finely tuned and powerful membrane perturbing system and mediator of inflammation. An overaggressive response, because of deficiency of CD46, will lead to excessive AP activity in the retina. This could both initiate and accelerate retinal and choroidal damage, resulting in the phenotype of *Cd46*$^{-/-}$ mice that closely resembles the dry form of human AMD.

We envision two scenarios as to how AMD could arise. From birth, these animals have reduced regulatory activity (a hyperinflammatory phenotype), which could initiate progressive damage to the predispositional ocular tissue. In other words, it is the primary (etiology) cause of the disease. A second possibility is that the gradual retinal degeneration and debris accumulation are parts of the aging process, being accelerated in the *Cd46*$^{-/-}$ mouse, and thus leading to earlier and more severe dry AMD-like changes.

In conclusion, our results provide powerful evidence that a defect in the local (ocular) control of the AP contributes to the etiopathogenesis of dry AMD. Selective tissue distribution of CD46 (only expressed by the inner acrosomal membrane of spermatozoa and in the eye) combined with the normal systemic AP activity gives the *Cd46*$^{-/-}$ model of dry AMD a unique advantage over other mouse models using knockout strains in the complement system. We are excited by the many possibilities of using this mouse model system in which the AP is intact, as it is in humans with AMD. Thus, the *Cd46*$^{-/-}$ mouse model could become a valuable tool in the investigation of dry AMD pathology and in analyzing potential targets to which complement-mediated therapy could be applied.

Thus, we propose that deficient ocular (local) complement regulation because of lack of CD46, in conjunction with an intact systemic AP, facilitates the development of dry AMD pathogenesis.

Acknowledgments

We thank Ruslana Tytarenko, Amy Cadis, and Robert Knox for technical assistance and helpful suggestions; and Prof. Brian P. Morgan (University of Wales College of Medicine) for providing polyclonal anti-MAC (C9 neoepitope) antibody.

Supplemental Data

Supplemental material for this article can be found at *http://dx.doi.org/10.1016/j.ajpath.2016.03.021*.

References

1. Friedman DS, O'Colmain BJ, Muñoz B, Tomany SC, McCarty C, de Jong PT, Nemesure B, Mitchell P, Kempen J: Prevalence of age-related macular degeneration in the United States. Arch Ophthalmol 2004, 122:564–572
2. Coleman HR, Chan CC, Ferris FL III, Chew EY: Age-related macular degeneration. Lancet 2008, 372:1835–1845

3. Gehrs KM, Anderson DH, Johnson LV, Hageman GS: Age-related macular degeneration: emerging pathogenetic and therapeutic concepts. Ann Med 2006, 38:450−471
4. Christoforidis JB, Tecce N, Dell'Omo R, Mastropasqua R, Verolino M, Costagliola C: Age related macular degeneration and visual disability. Curr Drug Targets 2011, 12:221−233
5. Rein DB, Wittenborn JS, Zhang X, Honeycutt AA, Lesesne SB, Saaddine J; Vision Health Cost-Effectiveness Study Group: Forecasting age-related macular degeneration through the year 2050: the potential impact of new treatments. Arch Ophthalmol 2009, 127: 533−540
6. Husain D, Ambati B, Adamis AP, Miller JW: Mechanisms of age-related macular degeneration. Ophthalmol Clin North Am 2002, 15: 87−91
7. Smith W, Assink J, Klein R, Mitchell P, Klaver CC, Klein BE, Hofman A, Jensen S, Wang JJ, de Jong PT: Risk factors for age-related macular degeneration: pooled findings from three continents. Ophthalmology 2001, 108:697−704
8. Evans JR: Risk factors for age-related macular degeneration. Prog Retin Eye Res 2001, 20:227−253
9. Khandhadia S, Cherry J, Lotery AJ: Age-related macular degeneration. Adv Exp Med Biol 2012, 724:15−36
10. Yates JR, Moore AT: Genetic susceptibility to age related macular degeneration. J Med Genet 2000, 37:83−87
11. Zarbin MA, Rosenfeld PJ: Pathway-based therapies for age-related macular degeneration: an integrated survey of emerging treatment alternatives. Retina 2010, 30:1350−1367
12. Querques G, Rosenfeld PJ, Cavallero E, Borrelli E, Corvi F, Querques L, Bandello FM, Zarbin MA: Treatment of dry age-related macular degeneration. Ophthalmic Res 2014, 52:107−115
13. Bora NS, Jha P, Lyzogubov VV, Bora PS: Emerging role of complement in ocular diseases. Curr Immunol Rev 2011, 7:360−367
14. Bora NS, Jha P, Bora PS: The role of complement in ocular pathology. Semin Immunopathol 2008, 30:85−95
15. Anderson DH, Radeke MJ, Gallo NB, Chapin EA, Johnson PT, Curletti CR, Hancox LS, Hu J, Ebright JN, Malek G, Hauser MA, Rickman CB, Bok D, Hageman GS, Johnson LV: The pivotal role of the complement system in aging and age-related macular degeneration: hypothesis re-visited. Prog Retin Eye Res 2010, 29: 95−112
16. Johnson LV, Leitner WP, Staples MK, Anderson DH: Complement activation and inflammatory processes in drusen formation and age related macular degeneration. Exp Eye Res 2001, 73:887−896
17. Seddon JM, Yu Y, Miller EC, Reynolds R, Tan PL, Gowrisankar S, Goldstein JI, Triebwasser M, Anderson HE, Zerbib J, Kavanagh D, Souied E, Katsanis N, Daly MJ, Atkinson JP, Raychaudhuri S: Rare variants in CFI, C3 and C9 are associated with high risk of advanced age-related macular degeneration. Nat Genet 2013, 45:1366−1370
18. Bora PS, Sohn JH, Cruz JM, Jha P, Nishihori H, Wang Y, Kaliappan S, Kaplan HJ, Bora NS: Role of complement and complement membrane attack complex in laser-induced choroidal neovascularization. J Immunol 2005, 174:491−497
19. Bora NS, Kaliappan S, Jha P, Cu Q, Sohn JH, Dhaulakhandi DB, Kaplan HJ, Bora PS: Complement activation via alternative pathway is critical in the development of laser-induced choroidal neovascularization: role of factor B and factor H. J Immunol 2006, 177: 1872−1878
20. Bora NS, Kaliappan S, Jha P, Xu Q, Sivasankar B, Harris CL, Morgan BP, Bora PS: CD59, a complement regulatory protein, controls choroidal neovascularization in a mouse model of wet-type age-related macular degeneration. J Immunol 2007, 178:1783−1790
21. Kaliappan S, Jha P, Lyzogubov VV, Tytarenko RG, Bora NS, Bora PS: Alcohol and nicotine consumption exacerbates choroidal neovascularization by modulating the regulation of complement system. FEBS Lett 2008, 582:3451−3458
22. Bora NS, Jha P, Lyzogubov VV, Kaliappan S, Liu J, Tytarenko RG, Fraser DA, Morgan BP, Bora PS: Recombinant membrane-targeted form of CD59 inhibits the growth of choroidal neovascular complex in mice. J Biol Chem 2010, 285:33826−33833
23. Lyzogubov VV, Tytarenko RG, Jha P, Liu J, Bora NS, Bora PS: Role of ocular complement factor H in a murine model of choroidal neovascularization. Am J Pathol 2010, 177:1870−1880
24. Lyzogubov VV, Tytarenko RG, Liu J, Bora NS, Bora PS: Polyethylene glycol (PEG)-induced mouse model of choroidal neovascularization. J Biol Chem 2011, 286:16229−16237
25. Liu J, Jha P, Lyzogubov VV, Tytarenko RG, Bora NS, Bora PS: Relationship between complement membrane attack complex, chemokine (C-C Motif) ligand 2 (CCL2) and vascular endothelial growth factor in mouse model of laser-induced choroidal neovascularization. J Biol Chem 2011, 286:20991−21001
26. Lyzogubov VV, Bora NS, Tytarenko RG, Bora PS: Polyethylene glycol induced mouse model of retinal degeneration. Exp Eye Res 2014, 127:143−152
27. Bora NS, Matta B, Lyzogubov VV, Bora PS: Relationship between the complement system, risk factors and prediction models in age-related macular degeneration. Mol Immunol 2015, 63:176−183
28. Lyzogubov V, Wu X, Jha P, Tytarenko R, Triebwasser M, Kolar G, Bertram P, Bora PS, Atkinson JP, Bora NS: Complement regulatory protein CD46 protects against choroidal neovascularization in mice. Am J Pathol 2014, 184:2537−2548
29. Liszewski MK, Atkinson JP: Regulatory proteins of complement. Edited by Volanakis J, Frank M. The Human Complement System in Health and Disease. New York: Marcel Dekker, 1998, pp 149−166
30. Morgan BP, Harris CL (Eds): Complement Regulatory Proteins. San Diego, London: Academic Press, 1999
31. Liszewski MK, Leung M, Cui W, Subramanian VB, Parkinson J, Barlow PN, Manchester M, Atkinson JP: Dissecting sites important for complement regulatory activity in membrane cofactor protein (MCP; CD46). J Biol Chem 2000, 275:37692−37701
32. Liszewski MK, Kemper C, Price JD, Atkinson JP: Emerging roles and new functions of CD46. Springer Semin Immunopathol 2005, 27: 345−358
33. Stover CM, Luckett JC, Echtenacher B, Dupont A, Figgitt SE, Brown J, Männel DN, Schwaeble WJ: Properdin plays a protective role in polymicrobial septic peritonitis. J Immunol 2008, 180:3313−3318
34. Circolo A, Garnier G, Fukuda W, Wang X, Hidvegi T, Szalai AJ, Briles DE, Volanakis JE, Wetsel RA, Colten HR: Genetic disruption of the murine complement C3 promoter region generates deficient mice with extrahepatic expression of C3 mRNA. Immunopharmacology 1999, 42:135−149
35. Matsumoto M, Fukuda W, Circolo A, Goellner J, Strauss-Schoenberger J, Wang X, Fujita S, Hidvegi T, Chaplin DD, Colten HR: Abrogation of the alternative complement pathway by targeted deletion of murine factor B. Proc Natl Acad Sci U S A 1997, 94:8720−8725
36. Bertram P, Akk AM, Zhou HF, Mitchell LM, Pham CT, Hourcade DE: Anti-mouse properdin TSR 5/6 monoclonal antibodies block complement alternative pathway-dependent pathogenesis. Monoclon Antib Immunodiagn Immunother 2015, 34:1−6
37. Ethen CM, Feng X, Olsen TW, Ferrington DA: Declines in arrestin and rhodopsin in the macula with progression of age-related macular degeneration. Invest Ophthalmol Vis Sci 2005, 46:769−775
38. Zhao Z, Chen Y, Wang J, Sternberg P, Freeman ML, Grossniklaus HE, Cai J: Age-related retinopathy in NRF2-deficient mice. PLoS One 2011, 6:e19456
39. Cho KS, Yoon YH, Choi JA, Lee SJ, Koh JY: Induction of autophagy and cell death by tamoxifen in cultured retinal pigment epithelial and photoreceptor cells. Invest Ophthalmol Vis Sci 2012, 53:5344−5353
40. Fujihara M, Bartels E, Nielsen LB, Handa JT: A human apoB100 transgenic mouse expresses human apoB100 in the RPE and develops features of early AMD. Exp Eye Res 2009, 88:1115−1123
41. Anderson DH, Mullins RF, Hageman GS, Johnson LV: A role for local inflammation in the formation of drusen in the aging eye. Am J Ophthalmol 2002, 134:411−431

42. Kaarniranta K, Kauppinen A, Blasiak J, Salminen A: Autophagy regulating kinases as potential therapeutic targets for age-related macular degeneration. Future Med Chem 2012, 4:2153–2161
43. Saint-Geniez M, Maldonado AE, D'Amore PA: VEGF expression and receptor activation in the choroid during development and in the adult. Invest Ophthalmol Vis Sci 2006, 47:3135–3142
44. Ramkumar HL, Zhang J, Chan CC: Retinal ultrastructure of murine models of dry age-related macular degeneration (AMD). Prog Retin Eye Res 2010, 29:169–190
45. Ambati J, Anand A, Fernandez S, Sakurai E, Lynn BC, Kuziel WA, Rollins BJ, Ambati BK: An animal model of age-related macular degeneration in senescent Ccl-2- or Ccr-2-deficient mice. Nat Med 2003, 9:1390–1397
46. Chader GJ: Animal models in research on retinal degenerations: past progress and future hope. Vision Res 2002, 42:393–399
47. Mata NL, Tzekov RT, Liu X, Weng J, Birch DG, Travis GH: Delayed dark-adaptation and lipofuscin accumulation in abcr+/- mice: implications for involvement of ABCR in age-related macular degeneration. Invest Ophthalmol Vis Sci 2001, 42:1685–1690
48. Wang AL, Neufeld AH: Smoking mice: a potential model for studying accumulation of drusen-like material on Bruch's membrane. Vision Res 2010, 50:638–642
49. Fujihara M, Nagai N, Sussan TE, Biswal S, Handa JT: Chronic cigarette smoke causes oxidative damage and apoptosis to retinal pigmented epithelial cells in mice. PLoS One 2008, 3:e3119
50. Fu L, Garland D, Yang Z, Shukla D, Rajendran A, Pearson E, Stone EM, Zhang K, Pierce EA: The R345W mutation in EFEMP1 is pathogenic and causes AMD-like deposits in mice. Hum Mol Genet 2007, 16:2411–2422
51. Coffey PJ, Gias C, McDermott CJ, Lundh P, Pickering MC, Sethi C, Bird A, Fitzke FW, Maass A, Chen LL, Holder GE, Luthert PJ, Salt TE, Moss SE, Greenwood J: Complement factor H deficiency in aged mice causes retinal abnormalities and visual dysfunction. Proc Natl Acad Sci U S A 2007, 104:16651–16656
52. Ufret-Vincenty RL, Aredo B, Liu X, McMahon A, Chen PW, Sun H, Niederkorn JY, Kedzierski W: Transgenic mice expressing variants of complement factor H develop AMD-like retinal findings. Invest Ophthalmol Vis Sci 2010, 51:5878–5887
53. Neuhardt T, May CA, Wilsch C, Eichhorn M, Lütjen-Drecoll E: Morphological changes of retinal pigment epithelium and choroid in rd-mice. Exp Eye Res 1999, 68:75–83
54. Karan G, Lillo C, Yang Z, Cameron DJ, Locke KG, Zhao Y, Thirumalaichary S, Li C, Birch DG, Vollmer-Snarr HR, Williams DS, Zhang K: Lipofuscin accumulation, abnormal electrophysiology, and photoreceptor degeneration in mutant ELOVL4 transgenic mice: a model for macular degeneration. Proc Natl Acad Sci U S A 2005, 102:4164–4169
55. Majji AB, Cao J, Chang KY, Hayashi A, Aggarwal S, Grebe RR, De Juan E Jr: Age-related retinal pigment epithelium and Bruch's membrane degeneration in senescence-accelerated mouse. Invest Ophthalmol Vis Sci 2000, 41:3936–3942
56. Luhmann UF, Robbie S, Munro PM, Barker SE, Duran Y, Luong V, Fitzke FW, Bainbridge JW, Ali RR, MacLaren RE: The drusenlike phenotype in aging Ccl2-knockout mice is caused by an accelerated accumulation of swollen autofluorescent subretinal macrophages. Invest Ophthalmol Vis Sci 2009, 50:5934–5943
57. Luhmann UF, Carvalho LS, Robbie SJ, Cowing JA, Duran Y, Munro PM, Bainbridge JW, Ali RR: Ccl2, Cx3cr1 and Ccl2/Cx3cr1 chemokine deficiencies are not sufficient to cause age-related retinal degeneration. Exp Eye Res 2013, 107:80–87
58. Chang B, Hawes NL, Hurd RE, Wang J, Howell D, Davisson MT, Roderick TH, Nusinowitz S, Heckenlively JR: Mouse models of ocular diseases. Vis Neurosci 2005, 22:587–593
59. Hadziahmetovic M, Dentchev T, Song Y, Haddad N, He X, Hahn P, Pratico D, Wen R, Harris ZL, Lambris JD, Beard J, Dunaief JL: Ceruloplasmin/hephaestin knockout mice model morphologic and molecular features of AMD. Invest Ophthalmol Vis Sci 2008, 49:2728–2736
60. Hafezi F, Grimm C, Simmen BC, Wenzel A, Remé CE: Molecular ophthalmology: an update on animal models for retinal degenerations and dystrophies. Br J Ophthalmol 2000, 84:922–927
61. Imamura Y, Noda S, Hashizume K, Shinoda K, Yamaguchi M, Uchiyama S, Shimizu T, Mizushima Y, Shirasawa T, Tsubota K: Drusen, choroidal neovascularization, and retinal pigment epithelium dysfunction in SOD1-deficient mice: a model of age-related macular degeneration. Proc Natl Acad Sci U S A 2006, 103:11282–11287
62. Ross RJ, Zhou M, Shen D, Fariss RN, Ding X, Bojanowski CM, Tuo J, Chan CC: Immunological protein expression profile in Ccl2/Cx3cr1 deficient mice with lesions similar to age-related macular degeneration. Exp Eye Res 2008, 86:675–683
63. Tuo J, Bojanowski CM, Zhou M, Shen D, Ross RJ, Rosenberg KI, Cameron DJ, Yin C, Kowalak JA, Zhuang Z, Zhang K, Chan CC: Murine ccl2/cx3cr1 deficiency results in retinal lesions mimicking human age-related macular degeneration. Invest Ophthalmol Vis Sci 2007, 48:3827–3836
64. Zeiss CJ: Animals as models of age-related macular degeneration: an imperfect measure of the truth. Vet Pathol 2010, 47:396–413
65. Justilien V, Pang JJ, Renganathan K, Zhan X, Crabb JW, Kim SR, Sparrow JR, Hauswirth WW, Lewin AS: SOD2 knockdown mouse model of early AMD. Invest Ophthalmol Vis Sci 2007, 48:4407–4420
66. Hashizume K, Hirasawa M, Imamura Y, Noda S, Shimizu T, Shinoda K, Kurihara T, Noda K, Ozawa Y, Ishida S, Miyake Y, Shirasawa T, Tsubota K: Retinal dysfunction and progressive retinal cell death in SOD1-deficient mice. Am J Pathol 2008, 172:1325–1331
67. Schmidt-Erfurth U, Rudolf M, Funk M, Hofmann-Rummelt C, Franz-Haas NS, Aherrahrou Z, Schlötzer-Schrehardt U: Ultrastructural changes in a murine model of graded Bruch membrane lipoidal degeneration and corresponding VEGF164 detection. Invest Ophthalmol Vis Sci 2008, 49:390–398
68. Espinosa-Heidmann DG, Sall J, Hernandez EP, Cousins SW: Basal laminar deposit formation in APO B100 transgenic mice: complex interactions between dietary fat, blue light, and vitamin E. Invest Ophthalmol Vis Sci 2004, 45:260–266
69. Malek G, Johnson LV, Mace BE, Saloupis P, Schmechel DE, Rickman DW, Toth CA, Sullivan PM, Bowes Rickman C: Apolipoprotein E allele-dependent pathogenesis: a model for age-related retinal degeneration. Proc Natl Acad Sci U S A 2005, 102:11900–11905
70. Sallo FB, Bereczki E, Csont T, Luthert PJ, Munro P, Ferdinandy P, Sántha M, Lengyel I: Bruch's membrane changes in transgenic mice overexpressing the human biglycan and apolipoprotein b-100 genes. Exp Eye Res 2009, 89:178–186
71. Elizabeth Rakoczy P, Yu MJ, Nusinowitz S, Chang B, Heckenlively JR: Mouse models of age-related macular degeneration. Exp Eye Res 2006, 82:741–752
72. Edwards AO, Malek G: Molecular genetics of AMD and current animal models. Angiogenesis 2007, 10:119–132
73. Bhutto I, Lutty G: Understanding age-related macular degeneration (AMD): relationships between the photoreceptor/retinal pigment epithelium/Bruch's membrane/choriocapillaris complex. Mol Aspects Med 2012, 33:295–317
74. Ambati J, Atkinson JP, Gelfand BD: Immunology of age-related macular degeneration. Nat Rev Immunol 2013, 13:438–451
75. Horie-Inoue K, Inoue S: Genomic aspects of age-related macular degeneration. Biochem Biophys Res Commun 2014, 452:263–275
76. Yu Y, Triebwasser MP, Wong EK, Schramm EC, Thomas B, Reynolds R, Mardis ER, Atkinson JP, Daly M, Raychaudhuri S, Kavanagh D, Seddon JM: Whole-exome sequencing identifies rare, functional CFH variants in families with macular degeneration. Hum Mol Genet 2014, 23:5283–5293
77. Kavanagh D, Yu Y, Schramm EC, Triebwasser M, Wagner EK, Raychaudhuri S, Daly MJ, Atkinson JP, Seddon JM: Rare genetic

variants in the CFI gene are associated with advanced age-related macular degeneration and commonly result in reduced serum factor I levels. Hum Mol Genet 2015, 24:3861–3870
78. Triebwasser MP, Roberson ED, Yu Y, Schramm EC, Wagner EK, Raychaudhuri S, Seddon JM, Atkinson JP: Rare variants in the functional domains of complement factor H are associated with age-related macular degeneration. Invest Ophthalmol Vis Sci 2015, 56: 6873–6878
79. Helgason H, Sulem P, Duvvari MR, Luo H, Thorleifsson G, Stefansson H, et al: A rare nonsynonymous sequence variant in C3 is associated with high risk of age-related macular degeneration. Nat Genet 2013, 45:1371–1374
80. Strauss O: The retinal pigment epithelium in visual function. Physiol Rev 2005, 85:845–881
81. Sparrow JR, Gregory-Roberts E, Yamamoto K, Blonska A, Ghosh SK, Ueda K, Zhou J: The bisretinoids of retinal pigment epithelium. Prog Retin Eye Res 2012, 31:121–135
82. Choi AM, Ryter SW, Levine B: Autophagy in human health and disease. N Engl J Med 2013, 368:651–662
83. Radu RA, Hu J, Jiang Z, Bok D: Bisretinoid-mediated complement activation on retinal pigment epithelial cells is dependent on complement factor H haplotype. J Biol Chem 2014, 289: 9113–9120
84. Wang AL, Lukas TJ, Yuan M, Du N, Tso MO, Neufeld AH: Autophagy and exosomes in the aged retinal pigment epithelium: possible relevance to drusen formation and age-related macular degeneration. PLoS One 2009, 4:e4160
85. Viiri J, Amadio M, Marchesi N, Hyttinen JM, Kivinen N, Sironen R, Rilla K, Akhtar S, Provenzani A, D'Agostino VG, Govoni S, Pascale A, Agostini H, Petrovski G, Salminen A, Kaarniranta K: Autophagy activation clears ELAVL1/HuR-mediated accumulation of SQSTM1/p62 during proteasomal inhibition in human retinal pigment epithelial cells. PLoS One 2013, 8:e69563
86. Spraul CW, Lang GE, Grossniklaus HE, Lang GK: Histologic and morphometric analysis of the choroid, Bruch's membrane, and retinal pigment epithelium in postmortem eyes with age-related macular degeneration and histologic examination of surgically excised choroidal neovascular membranes. Surv Ophthalmol 1999, 44(Suppl 1):S10–S32
87. Hageman GS, Gehrs K, Johnson LV, Anderson D: Age-Related Macular Degeneration (AMD): 2008 Jan 01 [Internet]. Edited by Kolb H, Fernandez E, Nelson R. In Webvision: The Organization of the Retina and Visual System. Salt Lake City (UT): University of Utah Health Sciences Center, 1995. Available at http://webvision.med.utah.edu/book/part-xii-cell-biology-of-retinal-degenerations/age-related-macular-degeneration-amd (accessed January 15, 2016)
88. Pickering MC, Cook HT, Warren J, Bygrave AE, Moss J, Walport MJ, Botto M: Uncontrolled C3 activation causes membranoproliferative glomerulonephritis in mice deficient in complement factor H. Nat Genet 2002, 31:424–428
89. Chang B, Hurd R, Wang J, Nishina P: Survey of common eye diseases in laboratory mouse strains. Invest Ophthalmol Vis Sci 2013, 54:4974–4981
90. Mehalow AK, Kameya S, Smith RS, Hawes NL, Denegre JM, Young JA, Bechtold L, Haider NB, Tepass U, Heckenlively JR, Chang B, Naggert JK, Nishina PM: CRB1 is essential for external limiting membrane integrity and photoreceptor morphogenesis in the mammalian retina. Hum Mol Genet 2003, 12:2179–2189